Integral Projection Models: Simulation Studies and Sensitivity Analyses

by

Kai Zhu

Department of Statistical Science
Duke University

Date:_____
Approved:

_____
Alan E. Gelfand, Supervisor

_____
Merlise A. Clyde

_____
James S. Clark

Thesis submitted in partial fulfillment of
the requirements for the degree of
Master of Science in the Department of Statistical Science
in the Graduate School of Duke University

2014

ABSTRACT

Integral Projection Models: Simulation Studies and Sensitivity Analyses

by

Kai Zhu

Department of Statistical Science
Duke University

Date:_____
Approved:

_____
Alan E. Gelfand, Supervisor

_____
Merlise A. Clyde

_____
James S. Clark

An abstract of a thesis submitted in partial fulfillment of
the requirements for the degree of
Master of Science in the Department of Statistical Science
in the Graduate School of Duke University

2014

Abstract

Integral projection model (IPM) is an important tool to study population dynamics and demography in ecology. Traditional IPMs are handled first with a fitting stage at individual-level transitions, then with a projection stage at population-level distributions. Here we adopt a new IPM framework that coherently focusing on population-level size distributions using point pattern theory.

We conduct simulation studies and sensitivity analyses to explore the properties of this new IPM framework. Under certain settings of demographic functions and parameters, we conduct two simulation studies by deterministically projecting population dynamics and stochastically generating point patterns. Assuming stationarity at equilibrium state, we then derive analytical solutions for the sensitivity of stable stage size distribution to kernel demographic parameters. We implement the sensitivity analyses to the two simulation studies. Demography, population dynamics, prior vs. posterior parameters, and sensitivities are compared among parameter settings and simulations.

For two simulation studies, we find that parameter recovery is challenging except under tight priors, suggesting possible parameter identification problems. Issues could somewhat be resolved by sensitivity analyses, which identify parameters that are most sensitive to the stable stage size distributions. In summary, we find population-level only data may be limited to infer demography, and we will integrate both individual- and population-level data in the future.

Contents

Abstract iv

List of Figures vi

Acknowledgements viii

1 Integral projection models: simulation studies and sensitivity analyses 1

1.1 Overview 1

1.1.1 Population dynamics and demography 1

1.1.2 Individual-level and population-level IPMs 3

1.2 Simulation studies 6

1.2.1 Deterministic demographic functions 6

1.2.2 Stochastic point patterns 8

1.3 Sensitivity analyses 9

1.3.1 General considerations 10

1.3.2 Eigenvalue derivatives 12

1.3.3 Kernel derivatives 13

1.4 Implementations and results 16

1.4.1 Simulation studies 16

1.4.2 Sensitivity analyses 24

1.5 Summary and future works 49

References 51

List of Figures

Figure 1: Simulation 1 demographic functions (a: survival function; b: growth function; c: recruitment function) and overall kernel (d). 17

Figure 2: Simulation 1 size distributions changing with time. Red line is the deterministic intensity (γ_t); black histogram is the stochastic point pattern (X_t). 20

Figure 3: Simulation 1 total population size changing with time. Red is the deterministic intensity (γ_t); black is the stochastic point pattern (X_t). 20

Figure 4: Simulation 2 demographic functions (a: survival function; b: growth function; c: recruitment function) and overall kernel (d). Symbolism follows Figure 1. 22

Figure 5: Simulation 2 size distributions changing with time. Symbolism follows Figure 2. 23

Figure 6: Simulation 2 total population size changing with time. Symbolism follows Figure 3… 24

Figure 7: Simulation 1 with tight priors on all parameters (Equation 36). Left: true (black), prior (blue), and posterior (red) parameter (θ) comparisons. Right: sensitivity of stable stage distribution to parameters ($dw/d\theta$, posterior mean: solid; 95% credible intervals: dashed lines). Panels are (a) survival parameter $\beta_0^{(s)}$; (b) survival parameter $\beta_x^{(s)}$; (c) growth parameter $\beta_0^{(g)}$; (d) growth parameter $\beta_x^{(g)}$; (e) growth parameter $\sigma^{(g)}$; (f) fecundity parameter $\beta_0^{(f)}$; and (g) recruitment parameter $\eta^{(r)}$. 30

Figure 8: Simulation 1 with vague priors on survival parameters and tight priors on others (Equation 37). Symbolism follows Figure 7. 32

Figure 9: Simulation 1 with vague priors on growth parameters and tight priors on others (Equation 38). Symbolism follows Figure 7. 34

Figure 10: Simulation 1 with vague priors on fecundity parameter and tight priors on others (Equation 39). Symbolism follows Figure 7. 36

Figure 11: Simulation 1 with vague priors on recruitment parameter and tight priors on others (Equation 40). Symbolism follows Figure 7. 38

Figure 12: Simulation 2 with tight priors on all parameters (Equation 36). Symbolism follows Figure 7. 41

Figure 13: Simulation 2 with vague priors on survival parameters and tight priors on others (Equation 37). Symbolism follows Figure 7. 43

Figure 14: Simulation 2 with vague priors on growth parameters and tight priors on others (Equation 38). Symbolism follows Figure 7. 45

Figure 15: Simulation 2 with vague priors on fecundity parameter and tight priors on others (Equation 39). Symbolism follows Figure 7. 47

Figure 16: Simulation 2 with vague priors on recruitment parameter and tight priors on others (Equation 40). Symbolism follows Figure 7. 49

Acknowledgements

I would like to acknowledge my committee, Alan Gelfand, Merlise Clyde, and Jim Clark, for their support and guidance in my research. This thesis is also inspired from the discussion with Aaron Berdanier, Andria Dawson, Souparno Ghosh, Joao Monteiro, and Erin Schliep.

1 Integral projection models: simulation studies and sensitivity analyses

1.1 Overview

1.1.1 Population dynamics and demography

Understanding how species populations change over time and interact with the environment are goals of population ecology. Population dynamics, or demography, is also a central topic in conservation biology, where population viability analysis (PVA) aims to predict the long-term probability of a species persisting in a given environment. Ecologists and conservation biologists are interested in questions like "Will the population go extinct?" and "Do specific life stages require more attention for management?" To answer these questions, projection models are widely used to forecast population dynamics and assess risk for conservation and management applications. Two types of models are primarily used: *matrix projection (or population) model (MPM)* and *integral projection model (IPM)*.

MPMs are the classical projection model in population ecology (Caswell, 2001). Suppose a population is described by a vector n_t, where each entry gives the number of individuals in each size class at time *t*. A generic MPM can be written as

$$n_{t+1} = An_t \qquad 1$$

which describes how the population structure changes from time *t* to *t* + 1 through the *population projection matrix A*. The construct of MPMs requires the population to be divided into discrete stage classes, as in population vectors and matrices. However, when classes are defined by a continuous variable, e.g., tree diameter, there are no natural breakpoints, and the division is artificial.

Recently, IPMs have been proposed as an improvement over MPMs for populations where demographic rates depend on a continuous variable (Easterling *et al.*, 2000; Ellner & Rees, 2006). By analogy, suppose a population is described by a *size distribution* $n_t(x)$, which represents the number of size-*x* individuals at time *t*. A generic IPM can be written as

$$n_{t+1}(y) = \int_{\Omega} K(y,x)\, n_t(x)\, dx \qquad 2$$

which describes the population size distribution changes from time *t* to *t* + 1 through the *population projection kernel* $K(y,x)$ with the integration over the set of all possible sizes Ω. A kernel for size transitions allows us to specify demographic changes through time without creating artificial, discrete classes.

Individuals in the population can make transitions in three ways: grow, survive, and reproduce. Of these, growth and survival are existing individuals staying in the same population pool, while reproduction is new individuals coming in as influx. In this analysis, we consider time-invariant transitions, i.e., growth, survival, and reproduction do not depend on time. Thus the kernel is comprised of several *demographic functions*: survival-growth and reproduction (fecundity-recruitment),

$$K(y,x) = s(x)\, g(y \mid x) + f \cdot r(y) \qquad 3$$

where $s(x)$ is the probability that an individual size *x* survives from time *t* to *t* + 1; $g(y \mid x)$ is the probability that an individual grows from size *x* at time *t* to size *y* at time *t* + 1; f is the total number of newborn individuals (fecundity) reproduced by individuals of size *x* at time *t*; $r(y)$ is the probability that these newborn individuals grow into size *y* at time *t* + 1.

1.1.2 Individual-level and population-level IPMs

The conventional method for IPM usually involves two steps: (i) fitting demographic functions (e.g., s, g, f, r) using individual-level data, and followed by (ii) plugging those functions into a kernel to project population dynamics. Individual-level data means measurements following tagged individuals through time; while population-level data means size distributions without individual identity through time. Hereafter we term it *individual-level IPM (IIPM).* This *inference-projection* approach causes incoherent problems because it uses individual-level data for a population-level model. In other words, the kernel constructed by individual transitions is used to project the long-term size distributions of the population. Implicitly it assumes that individual-level transitions describe the redistribution of sizes at the population level. Issues arise because the projection of population dynamics is unconstrained by the observed population size or growth. The problem is compounded by the fact that covariation among demographic functions is ignored and projection uncertainty is vague, since the parameterization of demographic functions is separated from kernel projection.

To overcome the inherent mismatch in scales, here we propose a new *full-inference* approach for IPM using population-level data to learn population-level demography (Ghosh *et al.*, 2012). Hereafter we term it *population-level IPM (PIPM)*. PIPM adopts the same generic specification (Equations 2 and 3), but it only uses population size distribution data without individual information. In other words, we view the observed size distribution as a point pattern over a bounded interval. PIPM is built as a three-stage hierarchical Bayesian model.

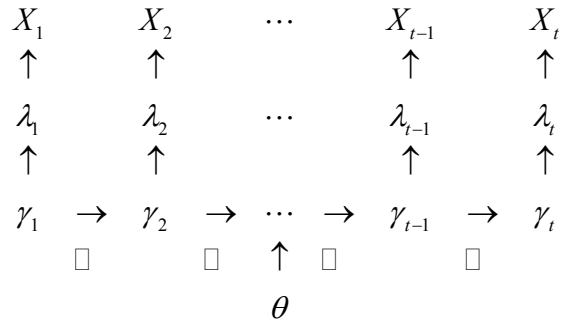

4

where X_t is the observed size distributions at time *t*; λ_t is the *density* at time *t* that generates point patterns through a nonhomogeneous Poisson process; γ_t is the *intensity* at time *t* that generates density through a log-scale Gaussian process, i.e., $\lambda_t = \gamma_t \exp(\varepsilon_t)$, where ε_t is a zero-mean Gaussian process; and γ_t is deterministically driven by a set of parameters θ through the kernel. The intensity $\gamma_t(x)$ changes with time by projecting and integrating the kernel $K(y,x)$ with multiple demographic functions (similar to Equation 3),

$$\begin{aligned}\gamma_{t+1}(y) &= \int_L^U K(y,x)\gamma_t(x)dx \\ &= \int_L^U \left(s(x)g(y\,|\,x) + f \cdot r(y)\right)\gamma_t(x)dx\end{aligned} \quad 5$$

where *L* and *U* are the lower and upper bounds of all possible sizes.

Here is a simple demonstration of how PIPM operates. The basic idea is to enumerate all possible paths for size transitions. Suppose there are three size classes (1, 2, 3). The intensity from time *t* to $t+1$ in the class 2 is obtained in the following fashion,

$$\begin{aligned}\gamma_{t+1}(2) = {} & l\left(s(1)g(2\,|\,1) + f \cdot r(2)\right)\gamma_t(1) \\ & + l\left(s(2)g(2\,|\,2) + f \cdot r(2)\right)\gamma_t(2) \\ & + l\left(s(3)g(2\,|\,3) + f \cdot r(2)\right)\gamma_t(3)\end{aligned} \quad 6$$

where l is the interval length of size class.

More generally, the computation of PIPM is implemented using the discretized versions of the projection kernel and size distribution,

$$\gamma_{t+1}(y_i) = l\sum_j \left(s(x_j)\, g(y_i \mid x_j) + f \cdot r(y_i)\right)\gamma_{t-1}(x_j) \qquad 7$$

where y_i, x_j are mid-points of the size class grid from L to U.

The result of an IPM is a collection of population statistics (population growth rate, population size distribution, etc.). These statistics depend on the kernel's functional forms and parameter values. Changing demographic parameters leads to change in population statistics. In this regard, *sensitivity analysis* quantifies how population statistics change by perturbing projection kernel. Sensitivity analysis could help to predict the results of future changes in the vital rates, quantify the effects of past changes, predict the action of natural selection, and design sampling schemes; thus it is "often more interesting, more robust, and more useful than the parameter estimates themselves." (Caswell, 2001, pp 206-207)

Population growth rate and size distribution are the two quantities of particular interest to population ecologists and conservation biologists. *Population growth rate* reflects the change of total population size which determines population viability (whether or not it is sustainable over time). *Population size distribution* reveals the relative density through size classes which determines population structure (whether or not it is dominated by small or large individuals). Following MPM theories, sensitivity analysis for IPM has been primarily focusing on population growth rate. Earlier developments involve sensitivity of population growth rate to kernel elements (Easterling *et al.*, 2000; Ellner & Rees, 2006); later developments shift to sensitivity of population growth rate to kernel parameters (Ellner & Rees, 2009). However, another equally

important population statistic—size distribution—has received little attention so far. Here we develop sensitivity analysis on population size distribution to kernel parameters.

To explore all these properties of PIPM, we conduct simulation studies and sensitivity analyses with prescribed parameters. The following sections first introduce parameter settings and algorithms for the simulation studies (1.2) and derive analytical solutions for the sensitivity analyses (1.3). We then describe computational implementations and summarize results (1.4). Finally, we conclude with summary and future works (1.5).

1.2 Simulation studies

The simulation studies are conducted in four steps: (i) select proper demographic functions for the projection kernel (functions in Equation 3); (ii) choose sensible parameters and initial size distributions; (iii) forward project deterministically population dynamics based on the discretized versions (Equation 7); and (iv) generate stochastic point pattern data from the deterministic projections.

1.2.1 Deterministic demographic functions

In simulations, the crucial step is to set up the demographic functions in the kernel. This step is purely deterministic, so the projections only depend on functions forms, parameter values, and initial size distributions. The kernel includes survival, growth, fecundity, and recruitment functions, whose settings are detailed below.

Survival function represents the probability of a certain size class to survive to the next time step. We use a logistic function of size x,

$$\text{logit}\left(s\left(x\right)\right) = \beta_0^{(s)} + \beta_x^{(s)} x \qquad 8$$

which can be rewritten as

$$s(x) = \frac{\exp\left(\beta_0^{(s)} + \beta_x^{(s)} x\right)}{1 + \exp\left(\beta_0^{(s)} + \beta_x^{(s)} x\right)} \tag{9}$$

Growth function represents the transition probability of a certain size class to grow to a different size class to the next time step. We use a truncated normal from lower (L) to upper (U) size bound,

$$y \mid x \sim \text{TruncatedNormal}\left(\mu(x), \sigma^2, L, U\right) \tag{10}$$

which can be rewritten as

$$g(y \mid x) = \begin{cases} \dfrac{\frac{1}{\sigma}\phi\left(\dfrac{y - \mu(x)}{\sigma}\right)}{\Phi\left(\dfrac{U - \mu(x)}{\sigma}\right) - \Phi\left(\dfrac{L - \mu(x)}{\sigma}\right)} & \text{for } y \in (L, U] \\ 0 & \text{otherwise} \end{cases} \tag{11}$$

where the mean is a linear function of size x,

$$\mu(x) = \beta_0^{(g)} + \beta_x^{(g)} x \tag{12}$$

Fecundity function represents the total number of newborn individuals, without respect to size classes. We use a positive constant for all sizes,

$$f = \exp\left(\beta_0^{(f)}\right) \tag{13}$$

which is parameterized on log scale for computational convenience.

Recruitment function represents the distribution of all newborn individuals (fecundity) to different size classes to the next time step. We use a truncated exponential from lower (L) to upper (U) size bound,

$$y \sim \text{TruncatedExponential}\left(\eta^{(r)}, L, U\right) \tag{14}$$

which can be rewritten as

$$r(y) = \begin{cases} \dfrac{\eta^{(r)} \exp\left(-\eta^{(r)} y\right)}{\exp\left(-\eta^{(r)} L\right) - \exp\left(-\eta^{(r)} U\right)} & \text{for } y \in (L, U] \\ 0 & \text{otherwise} \end{cases} \tag{15}$$

where $\eta^{(r)}$ is the rate parameter, controlling for the shape of the distribution.

In total, there are seven parameters $\theta = \left\{\beta_0^{(s)}, \beta_x^{(s)}, \beta_0^{(g)}, \beta_x^{(g)}, \sigma^{(g)}, \beta_0^{(f)}, \eta^{(r)}\right\}$ for all demographic functions.

1.2.2 Stochastic point patterns

We generate the stochastic point patterns based on the deterministic projections. We simplify the model (Equation 4) by simulating point patterns directly from the deterministic intensities.

$$\begin{array}{ccccccccccc} X_1 & & X_2 & & \cdots & & X_{t-1} & & X_t \\ \uparrow & & \uparrow & & & & \uparrow & & \uparrow \\ \gamma_1 & \rightarrow & \gamma_2 & \rightarrow & \cdots & \rightarrow & \gamma_{t-1} & \rightarrow & \gamma_t \\ & \square & & \square & \uparrow & \square & & \square & \\ & & & & \theta & & & & \end{array} \tag{16}$$

where γ_t's are simulated using Equation 5 with demographic functions in Equations 8 – 15. The integration is approximated by binning the continuous size distributions and matrix multiplication (Equation 7).

Given the deterministic intensities (γ_t), the stochastic point patterns (X_t) are generated using the rejection sampling technique for non-homogeneous Poisson process. It is implemented via the following thinning algorithm (Lewis & Shedler, 1979).

1. For n bins of the intensities $\gamma(x_1), \gamma(x_2), \ldots, \gamma(x_n)$, obtain the maximum bin intensity $\gamma_{\max} = \max\{\gamma(x_i), i = 1, 2, \ldots, n\}$.
2. Generate point patterns from a homogeneous Poisson with rate $\gamma_{\max}$, by sampling $N \sim \text{Poisson}(n \cdot \gamma_{\max})$ and random numbers $X_j \sim \text{Uniform}(L, U), j = 1, 2, \ldots N$.
3. Distribute X_j into the n bins; and for each bin i, accept X_j with probability $\frac{\gamma(x_i)}{\gamma_{\max}}$. These thinned $\{X_j\}$ are the realized point pattern of the non-homogeneous Poisson process.

1.3 Sensitivity analyses

The purpose of the sensitivity analysis is to understand how the projected population dynamics change with parameters. Given the deterministic kernel, analytical solutions can be obtained for sensitivity for each parameter. Therefore, the sensitivity analyses are conducted in two steps: (i) fit the model from the simulation studies; and (ii) implement sensitivity analyses on posterior samples of the fitted parameters and kernels. The model is fitted in Bayesian framework using R version 3.0.0 (R Development Core Team, 2013) with contributed package "pipm" (J.V.D. Monteiro, unpublished data). The sensitivity is then calculated using the following analytical solutions.

1.3.1 General considerations

Since the kernel is invariant to time, the PIPM is stationary for a stable population at the equilibrium state. Under this circumstance, the kernel can be discretized into a $m \times m$ matrix, where there are *m* discretized size classes. The discretized PIPM at equilibrium has a solution in the eigensystem of that matrix,

$$K(\theta)w(\theta) = \lambda(\theta)w(\theta) \qquad 17$$

where *K* is the discretized kernel, *w* is the discretized *stable stage distribution*, and λ is the *stable stage population growth rate*; all change with respect to (w.r.t.) parameters θ in the kernel.

The interest lies in how the stable stage distribution changes with the perturbation in the parameters of the discretized kernel, $dw/d\theta$. Take total derivative in Equation 17,

$$\left(dK(\theta)\right)w(\theta) + K(\theta)dw(\theta) = \lambda(\theta)dw(\theta) + w(\theta)d\lambda(\theta) \qquad 18$$

Rearranging,

$$dw(\theta) = \left(\lambda(\theta)I_m - K(\theta)\right)^{+}\left(\left(dK(\theta)\right)w(\theta) - w(\theta)d\lambda(\theta)\right) \qquad 19$$

where A^{+} is the Moore-Penrose pseudoinverse of *A*. Pseudoinverse is used because the matrix $\left(\lambda(\theta)I_m - K(\theta)\right)$ is singular.

The sensitivity of stable stage distribution w.r.t. parameters is obtained in the discretized kernel,

$$s_\theta = \frac{dw(\theta)}{d\theta^T} = \left(\lambda(\theta) I_m - K(\theta)\right)^+ \left(\frac{\left(dK(\theta)\right) w(\theta)}{d\theta^T} - w(\theta) \frac{d\lambda(\theta)}{d\theta^T} \right) \qquad 20$$

where $\theta^T = \left[\beta_0^{(s)}, \beta_x^{(s)}, \beta_0^{(g)}, \beta_x^{(g)}, \sigma^{(g)}, \beta_0^{(f)}, \eta^{(r)} \right]$ is a $1 \times p$ vector containing all parameters in Equations 8 – 15 . The sensitivity s_θ is a $m \times p$ matrix with entries $\left\{ \frac{\partial w_i}{\partial \theta_k} \right\}$.

Equation 20 can be simplified first by vectorizing *K* in the differentiation,

$$\begin{aligned} \left(dK(\theta)\right) w(\theta) &= \mathrm{vec}\left(I_m \left(dK(\theta)\right) w(\theta) \right) \\ &= \left(w(\theta)^T \otimes I_m \right) \mathrm{vec}\left(dK(\theta)\right) \\ &= \left(w(\theta)^T \otimes I_m \right) d\left(\mathrm{vec}\, K(\theta)\right) \end{aligned} \qquad 21$$

where $\otimes$ denotes Kronecker product.

To summarize, we have

$$s_\theta = \frac{dw(\theta)}{d\theta^T} = \left(\lambda(\theta) I_m - K(\theta)\right)^+ \left(\left(w(\theta)^T \otimes I_m \right) \frac{d\left(\mathrm{vec}\, K(\theta)\right)}{d\theta^T} - w(\theta) \frac{d\lambda(\theta)}{d\theta^T} \right) \qquad 22$$

where s_θ is a $m \times p$ matrix, $\left(\lambda(\theta) I_m - K(\theta)\right)^+$ is a $m \times m$ matrix, $\left(w(\theta)^T \otimes I_m \right)$ is a $m \times m^2$ matrix, $\frac{d\left(\mathrm{vec}\, K(\theta)\right)}{d\theta^T}$ is a $m^2 \times p$ matrix, $w(\theta)$ is a $m \times 1$ vector, and $\frac{d\lambda(\theta)}{d\theta^T}$ is a $1 \times p$ vector. Computations are detailed in the following sections.

1.3.2 Eigenvalue derivatives

This section deals with the computation of the eigenvalue derivatives, $\frac{d\lambda(\theta)}{d\theta^T}$. These derivatives are essentially the gradient vector of $\lambda(\theta)$, written as

$$\frac{d\lambda(\theta)}{d\theta^T} = \nabla\lambda(\theta) \qquad 23$$

Since $\lambda(\theta)$ is not tractable analytically, the gradient $\nabla\lambda(\theta)$ has to be evaluated numerically. Numerical gradients need to be calculated for the change of $\lambda(\theta)$ over a grid in θ space. However, due to the high dimensionality of θ space and complex nature of $\lambda(\theta)$, the only reasonable calculation would be to obtain local finite differences for a given θ_k, the k^{th} element in θ vector. For θ_k, perturb a small amount h_k, and the k^{th} element of the gradient is

$$\nabla\lambda(\theta)_k = \lim_{h_k \to 0} \frac{\lambda(\theta_k + h_k) - \lambda(\theta_k)}{h_k} \qquad 24$$

Note that for each k^{th} element, the change of $\lambda(\theta)_k$ might be of different order. A range of small perturbation h_k should be explored to ensure the accuracy of the numerical approximation. We tried different perturbations based on the MCMC standard deviation (SD) of the posterior parameters θ. We found 1 SD is generally robust and accurate for the computation.

1.3.3 Kernel derivatives

This section deals with the computation of the kernel derivatives $\frac{d\left(\mathrm{vec}\,K\left(\theta\right)\right)}{d\theta^T}$, by providing analytical solutions to each parameter.

In our IPM settings, for each pair of size transitions from x_j to y_i, the kernel is written as

$$K\left(y_i,x_j;\theta\right)=s\left(x_j;\beta_0^{(s)},\beta_x^{(s)}\right)g\left(y_i,x_j;\beta_0^{(g)},\beta_x^{(g)},\sigma^{(g)}\right)+f\left(\beta_0^{(f)}\right)r\left(y_i;\eta^{(r)}\right) \qquad 25$$

Thus the matrix differential is a collection of partial derivatives for the k^{th} parameter θ_k,

$$\frac{d\left(\mathrm{vec}\,K\left(\theta\right)\right)}{d\theta^T}=\left\{\frac{\partial K_{ij}}{\partial\theta_k}\right\} \qquad 26$$

The analytical solutions are derived as follows.

For the survival component,

$$\begin{aligned}\frac{\partial K_{ij}}{\partial\beta_0^{(s)}}&=\frac{\partial s\left(x_j;\beta_0^{(s)},\beta_x^{(s)}\right)}{\partial\beta_0^{(s)}}g\left(y_i,x_j;\beta_0^{(g)},\beta_x^{(g)},\sigma^{(g)}\right)\\&=g\left(y_i,x_j;\beta_0^{(g)},\beta_x^{(g)},\sigma^{(g)}\right)\frac{\partial s\left(x_j;\beta_0^{(s)},\beta_x^{(s)}\right)}{\partial\left(\beta_0^{(s)}+\beta_x^{(s)}x_j\right)}\frac{\partial\left(\beta_0^{(s)}+\beta_x^{(s)}x_j\right)}{\partial\beta_0^{(s)}}\\&=g\left(y_i,x_j;\beta_0^{(g)},\beta_x^{(g)},\sigma^{(g)}\right)\frac{\partial s\left(x_j;\beta_0^{(s)},\beta_x^{(s)}\right)}{\partial\left(\beta_0^{(s)}+\beta_x^{(s)}x_j\right)}\\&=g\left(y_i,x_j;\beta_0^{(g)},\beta_x^{(g)},\sigma^{(g)}\right)\frac{\exp\left(\beta_0^{(s)}+\beta_x^{(s)}x_j\right)}{\left(1+\exp\left(\beta_0^{(s)}+\beta_x^{(s)}x_j\right)\right)^2}\end{aligned} \qquad 27$$

$$\begin{aligned}\frac{\partial K_{ij}}{\partial \beta_x^{(s)}} &= \frac{\partial s\left(x_j;\beta_0^{(s)},\beta_x^{(s)}\right)}{\partial \beta_x^{(s)}} g\left(y_i,x_j;\beta_0^{(g)},\beta_x^{(g)},\sigma^{(g)}\right) \\ &= g\left(y_i,x_j;\beta_0^{(g)},\beta_x^{(g)},\sigma^{(g)}\right)\frac{\partial s\left(x_j;\beta_0^{(s)},\beta_x^{(s)}\right)}{\partial\left(\beta_0^{(s)}+\beta_x^{(s)}x_j\right)}\frac{\partial\left(\beta_0^{(s)}+\beta_x^{(s)}x_j\right)}{\partial \beta_x^{(s)}} \\ &= x_j\frac{\partial K_{ij}}{\partial \beta_0^{(s)}}\end{aligned} \tag{28}$$

For the growth component,

$$\begin{aligned}\frac{\partial K_{ij}}{\partial \beta_0^{(g)}} &= s\left(x_j;\beta_0^{(s)},\beta_x^{(s)}\right)\frac{\partial g\left(y_i,x_j;\beta_0^{(g)},\beta_x^{(g)},\sigma^{(g)}\right)}{\partial \beta_0^{(g)}} \\ &= s\left(x_j;\beta_0^{(s)},\beta_x^{(s)}\right)\frac{\partial g\left(y_i,x_j;\beta_0^{(g)},\beta_x^{(g)},\sigma^{(g)}\right)}{\partial \mu\left(x_j;\beta_0^{(g)},\beta_x^{(g)}\right)}\frac{\partial \mu\left(x_j;\beta_0^{(g)},\beta_x^{(g)}\right)}{\partial \beta_0^{(g)}} \\ &= s\left(x_j;\beta_0^{(s)},\beta_x^{(s)}\right)\frac{\partial g\left(y_i,x_j;\beta_0^{(g)},\beta_x^{(g)},\sigma^{(g)}\right)}{\partial \mu\left(x_j;\beta_0^{(g)},\beta_x^{(g)}\right)} \\ &= s\left(x_j;\beta_0^{(s)},\beta_x^{(s)}\right)\frac{1}{\sigma^2}\frac{\phi\left(\frac{y_i-\mu}{\sigma}\right)}{\left(\Phi\left(\frac{U-\mu}{\sigma}\right)-\Phi\left(\frac{L-\mu}{\sigma}\right)\right)^2} \\ &\times\left(\left(\frac{y_i-\mu}{\sigma}\right)\left(\Phi\left(\frac{U-\mu}{\sigma}\right)-\Phi\left(\frac{L-\mu}{\sigma}\right)\right)+\phi\left(\frac{U-\mu}{\sigma}\right)-\phi\left(\frac{L-\mu}{\sigma}\right)\right)\end{aligned} \tag{29}$$

Note that Equation 29 makes use of the fact that

$$\frac{d\Phi(t)}{dt}=\phi(t),\frac{d\phi(t)}{dt}=-t\phi(t) \tag{30}$$

The other parameters are

$$\begin{aligned}\frac{\partial K_{ij}}{\partial \beta_x^{(g)}} &= s\left(x_j;\beta_0^{(s)},\beta_x^{(s)}\right)\frac{\partial g\left(y_i,x_j;\beta_0^{(g)},\beta_x^{(g)},\sigma^{(g)}\right)}{\partial \beta_x^{(g)}} \\ &= s\left(x_j;\beta_0^{(s)},\beta_x^{(s)}\right)\frac{\partial g\left(y_i,x_j;\beta_0^{(g)},\beta_x^{(g)},\sigma^{(g)}\right)}{\partial \mu\left(x_j;\beta_0^{(g)},\beta_x^{(g)}\right)}\frac{\partial \mu\left(x_j;\beta_0^{(g)},\beta_x^{(g)}\right)}{\partial \beta_x^{(g)}} \\ &= s\left(x_j;\beta_0^{(s)},\beta_x^{(s)}\right)\frac{\partial g\left(y_i,x_j;\beta_0^{(g)},\beta_x^{(g)},\sigma^{(g)}\right)}{\partial \mu\left(x_j;\beta_0^{(g)},\beta_x^{(g)}\right)}x_j \\ &= x_j\frac{\partial K_{ij}}{\partial \beta_0^{(g)}}\end{aligned} \qquad 31$$

$$\begin{aligned}\frac{\partial K_{ij}}{\partial \sigma} &= s\left(x_j;\beta_0^{(s)},\beta_x^{(s)}\right)\frac{\partial g\left(y_i,x_j;\beta_0^{(g)},\beta_x^{(g)},\sigma^{(g)}\right)}{\partial \sigma} \\ &= s\left(x_j;\beta_0^{(s)},\beta_x^{(s)}\right)\frac{1}{\sigma^2}\frac{\phi\left(\frac{y_i-\mu}{\sigma}\right)}{\left(\Phi\left(\frac{U-\mu}{\sigma}\right)-\Phi\left(\frac{L-\mu}{\sigma}\right)\right)^2} \\ &\times\left(\left(-1+\left(\frac{y_i-\mu}{\sigma}\right)^2\right)\left(\Phi\left(\frac{U-\mu}{\sigma}\right)-\Phi\left(\frac{L-\mu}{\sigma}\right)\right)+\frac{1}{\sigma}\left((U-\mu)\phi\left(\frac{U-\mu}{\sigma}\right)-(L-\mu)\phi\left(\frac{L-\mu}{\sigma}\right)\right)\right)\end{aligned} \qquad 32$$

For the fecundity component,

$$\begin{aligned}\frac{\partial K_{ij}}{\partial \beta_0^{(f)}} &= \frac{\partial f\left(\beta_0^{(f)}\right)}{\partial \beta_0^{(f)}}r\left(y_i;\beta_0^{(r)}\right) \\ &= r\left(y_i;\beta_0^{(r)}\right)\exp\left(\beta_0^{(f)}\right)\end{aligned} \qquad 33$$

For the recruitment component,

$$\begin{aligned}\frac{\partial K_{ij}}{\partial \eta^{(r)}} &= f\left(\beta_0^{(f)}\right)\frac{\partial r\left(y_i;\eta^{(r)}\right)}{\partial \eta^{(r)}} \\ &= f\left(\beta_0^{(f)}\right)\frac{\left(1-\eta y+\eta L\right)e^{-\eta\left(y_i+L\right)}-\left(1-\eta y+\eta U\right)e^{-\eta\left(y_i+U\right)}}{\left(e^{-\eta L}-e^{-\eta U}\right)^2}\end{aligned} \qquad 34$$

In sum, the kernel derivatives are obtained by plugging Equations 27 – 34 to Equation 26,

$$\frac{d\left(\mathrm{vec}\,K\left(\theta\right)\right)}{d\theta^T}=\left\{\frac{\partial K_{ij}}{\partial \theta_k}\right\}=\left\{\frac{\partial K_{ij}}{\partial \beta_0^{(s)}},\frac{\partial K_{ij}}{\partial \beta_x^{(s)}},\frac{\partial K_{ij}}{\partial \beta_0^{(g)}},\frac{\partial K_{ij}}{\partial \beta_x^{(g)}},\frac{\partial K_{ij}}{\partial \sigma^{(g)}},\frac{\partial K_{ij}}{\partial \beta_0^{(f)}},\frac{\partial K_{ij}}{\partial \eta^{(r)}}\right\} \qquad 35$$

Finally, the sensitivity of stable stage distribution w.r.t. parameters (Equation 22) is integrated with eigenvalue derivatives (Equation 24) and kernel derivatives (Equation 35).

1.4 Implementations and results

We conduct two simulation studies, fit the simulated data, and implement the sensitivity analyses. This section presents implementations and results based on these two simulations.

1.4.1 Simulation studies

The parameters for two simulations are chosen to meet the criteria that demographic functions are sensible and the population growth rate is close to 1 (stationary). For size scale, we use 50 bins with lower $L=0$ and upper $U=10$ limits. We simulate 30 time steps.

Simulation 1—Motivated by a previous study on sagebrush data in Idaho (Dalgleish *et al.*, 2011), we set up a scenario with high survival rate ($\beta_0^{(s)}=2.26,\beta_x^{(s)}=0.23$), moderate growth rate ($\beta_0^{(g)}=0,\beta_x^{(g)}=1,\sigma^{(g)}=0.5$), low fecundity ($\beta_0^{(f)}=-2.6$), and recruitment rate rapidly declining with size ($\eta^{(r)}=10$). Figure 1 shows survival rates range from 0.9 to 1; growth

rates peak along the diagonal of the size transition kernel; recruitment rates drop off quickly at small sizes; and the overall kernel is largely determined by the survival-growth and replenished by the fecundity-recruitment.

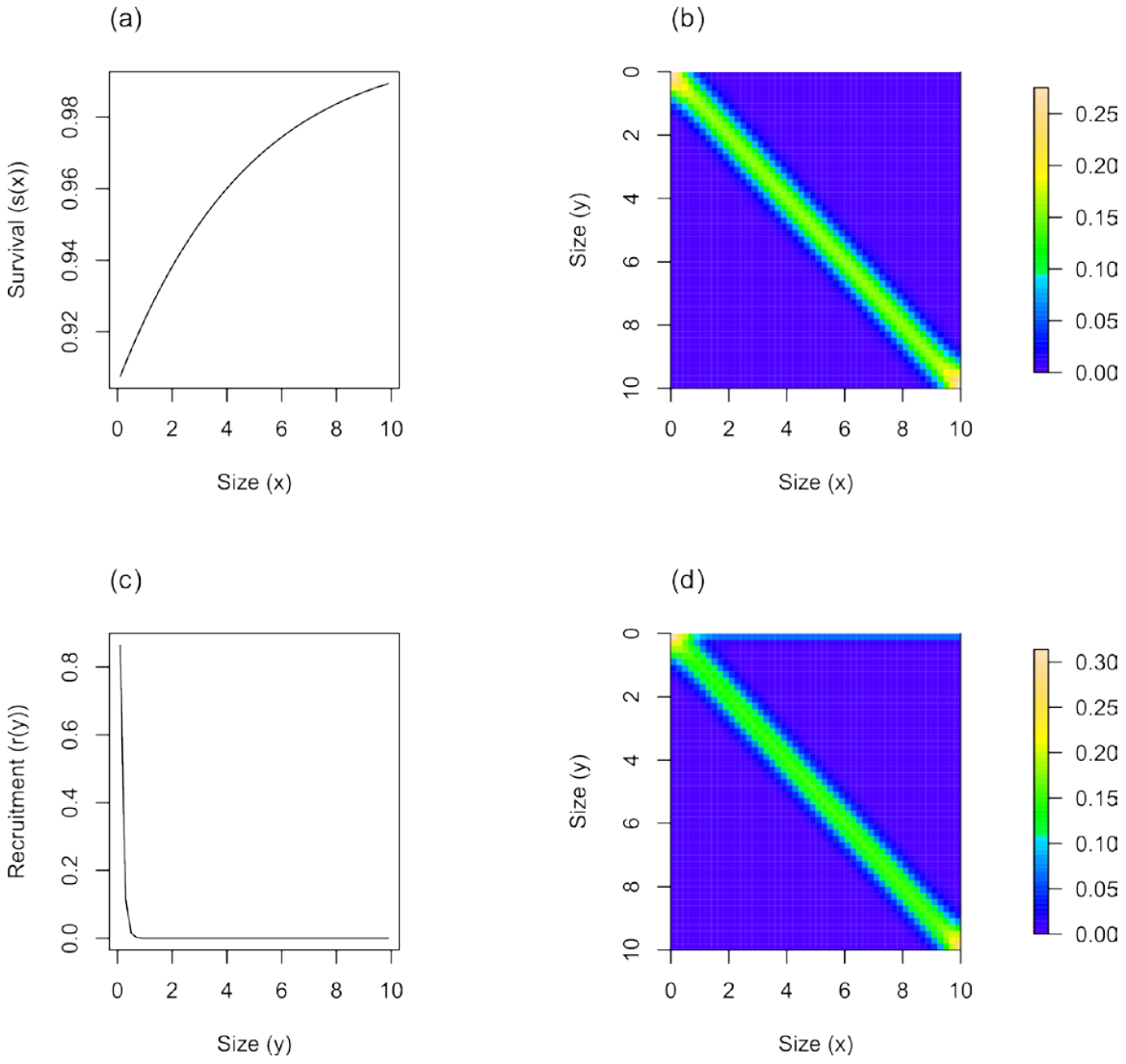

Figure 1: Simulation 1 demographic functions (a: survival function; b: growth function; c: recruitment function) and overall kernel (d).

To simulate point patterns, we set the initial values as the observed size distributions of the sagebrush data (Dalgleish *et al.*, 2011). Through 30 time steps, simulation shows that size

distributions gradually shifting to small sizes because of little growth; the total population size is maintained by fecundity-recruitment; the population size distribution stabilizes with individuals concentrating on small sizes (Figure 2).

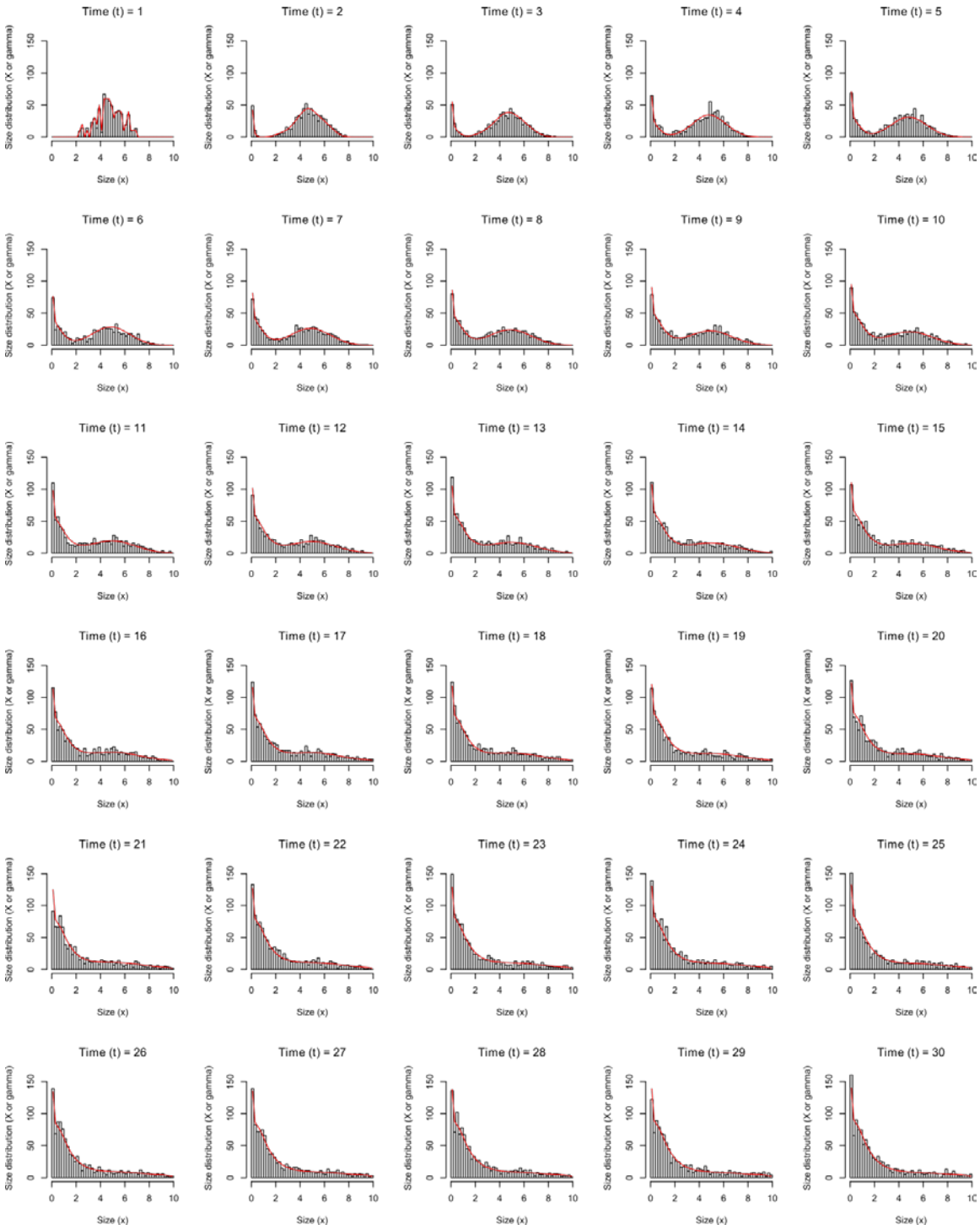
Time (t) = 1
Time (t) = 2
Time (t) = 3
Time (t) = 4
Time (t) = 5
Time (t) = 6
Time (t) = 7
Time (t) = 8
Time (t) = 9
Time (t) = 10
Time (t) = 11
Time (t) = 12
Time (t) = 13
Time (t) = 14
Time (t) = 15
Time (t) = 16
Time (t) = 17
Time (t) = 18
Time (t) = 19
Time (t) = 20
Time (t) = 21
Time (t) = 22
Time (t) = 23
Time (t) = 24
Time (t) = 25
Time (t) = 26
Time (t) = 27
Time (t) = 28
Time (t) = 29
Time (t) = 30
Size distribution (X or gamma)
Size (x)

Figure 2: Simulation 1 size distributions changing with time. Red line is the deterministic intensity (γ_t); black histogram is the stochastic point pattern (X_t).

The total population size gradually increases through the 30 time steps (Figure 3). In fact, the dominant eigenvalue of the kernel is 1.004, which determines the ergodic properties of population growth.

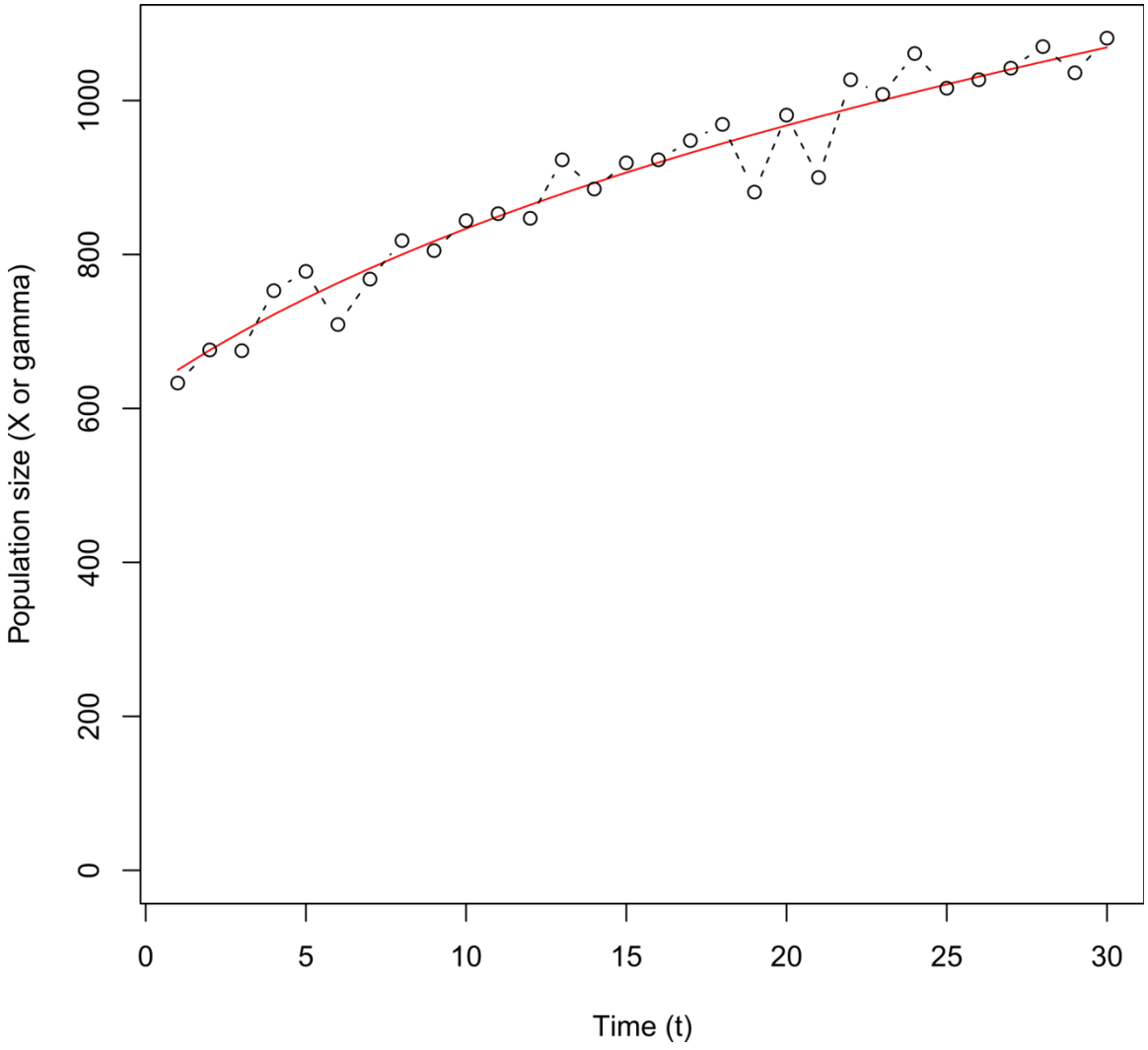

Figure 3: Simulation 1 total population size changing with time. Red is the deterministic intensity (γ_t); black is the stochastic point pattern (X_t).

Simulation 2—To exploit the information from changing size distributions, we set up an extreme scenario that has the maximal amount of dynamics of transition distribution, with rapid growth for small initial size distributions. The demographic parameters are set as moderate survival rate ($\beta_0^{(s)} = 0, \beta_x^{(s)} = 0.3$), high growth rate ($\beta_0^{(g)} = 1.1, \beta_x^{(g)} = 1, \sigma^{(g)} = 0.1$), moderate fecundity ($\beta_0^{(f)} = -1.2$), and recruitment moderately declining with size ($\eta^{(r)} = 3$). Figure 4 shows that survival rates range from 0.5 to 0.95; growth rates peak at larger sizes; recruitment rates drop off at small sizes; and the overall kernel is largely determined by the survival-growth and replenished by the fecundity-recruitment.

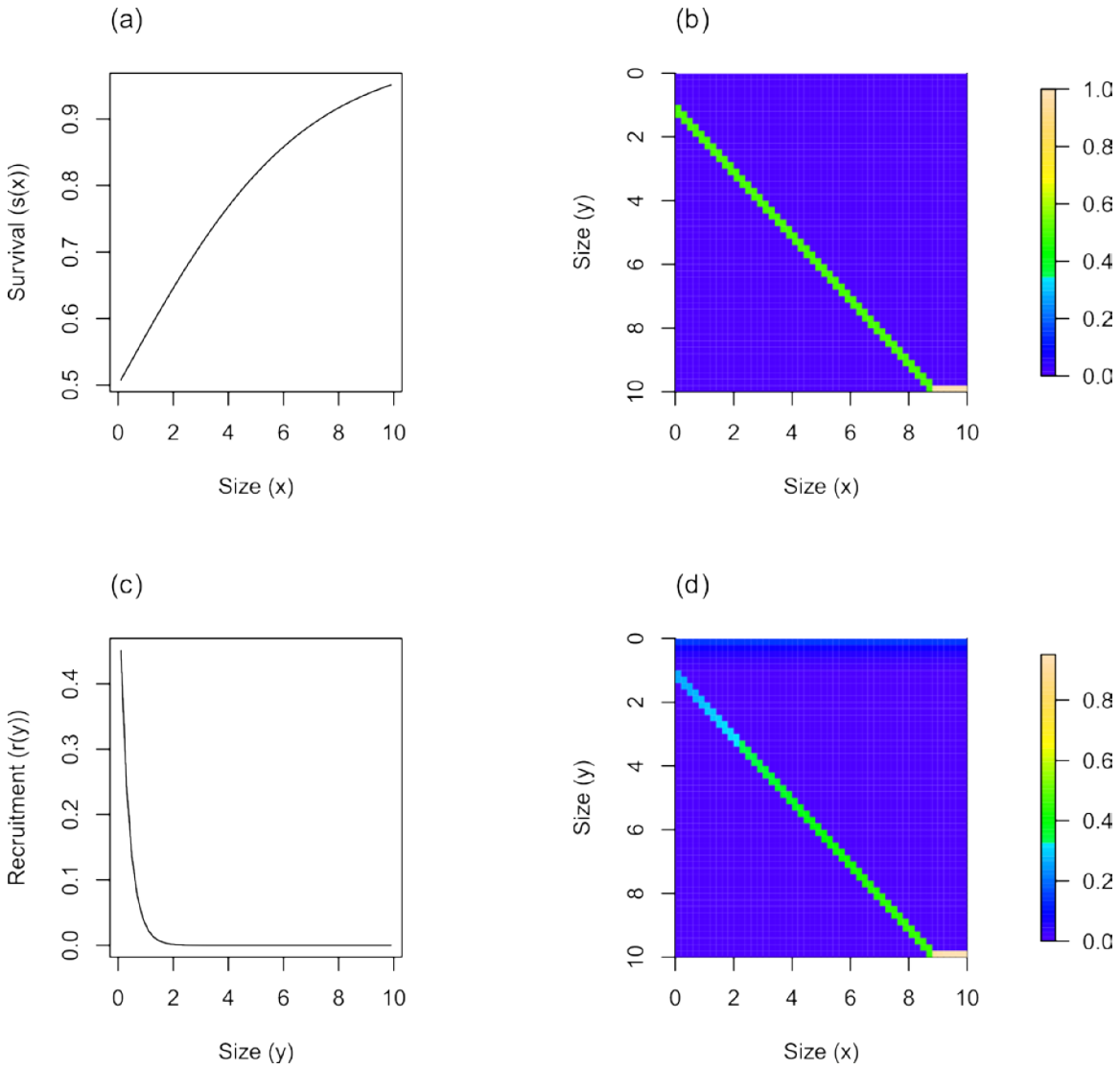

Figure 4: Simulation 2 demographic functions (a: survival function; b: growth function; c: recruitment function) and overall kernel (d). Symbolism follows Figure 1.

To simulate point patterns, we set the initial values concentrating at small sizes. Through 30 time steps, simulation shows that size distributions rapidly shifting to large sizes, i.e., growth. The accumulation in the largest size class is due to the truncated normal distribution (Figure 5).

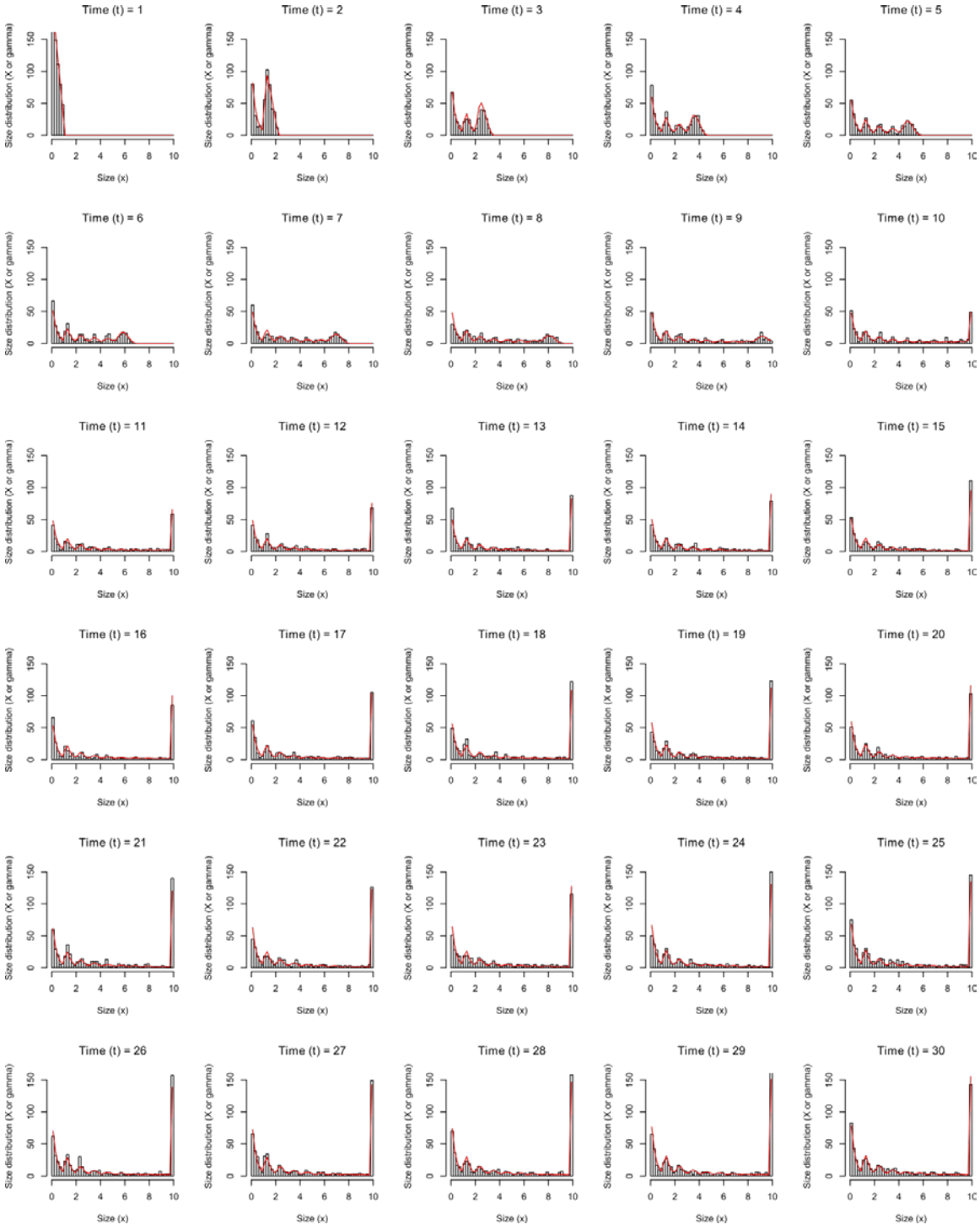

Figure 5: Simulation 2 size distributions changing with time. Symbolism follows Figure 2.

The total population size decreases first and then gradually increases through the 30 time steps (Figure 6). The dominant eigenvalue of the kernel is 1.028.

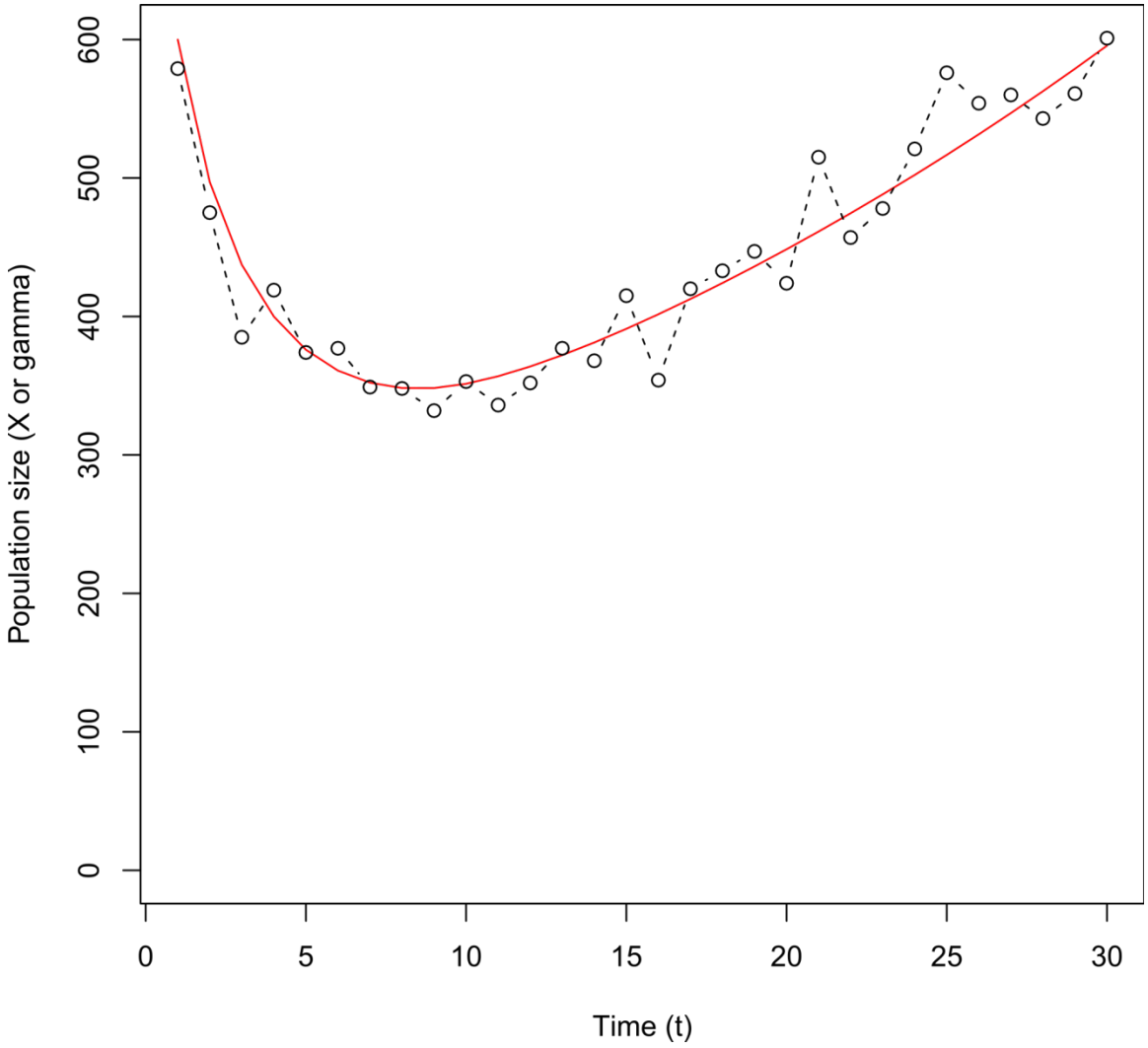

Figure 6: Simulation 2 total population size changing with time. Symbolism follows Figure 3.

1.4.2 Sensitivity analyses

We fit the model in Bayesian framework using R version 3.0.0 (R Development Core Team 2013) with contributed package "pipm" (J.V.D. Monteiro, unpublished data). The PIPM

has posterior samples of the parameter vector $\theta^{(g)}$. We can then calculate the discretized kernel $K^{(g)}$, and perform an eigenanalysis to obtain the eigenvalue $\lambda^{(g)}$ and eigenvector $w^{(g)}$. The sensitivity of Equation 22 integrates calculations from Equations 26 – 34 and 24.

For the two simulation data sets, we fit the model using the following prior settings. The rationale is first to impose tight priors on all parameters, centered on true values with small uncertainty; then to release priors, with uninformative distributions, on parameters in each component (survival, growth, fecundity, and recruitment) one by one. Priors for the location parameters ($\beta_0^{(s)}, \beta_x^{(s)}, \beta_0^{(g)}, \beta_x^{(g)}, \beta_0^{(f)}$) are normal distributions, except truncated normal distributions with the constraints on $\beta_x^{(s)} > 0$ and $\beta_x^{(g)} > 0$. Priors for the scale parameters ($\sigma^{(g)}, \eta^{(r)}$) are uniform distributions. The specific settings are detailed as follows.

1. Tight priors on all parameters, which centered on true values.

$$\begin{aligned}
\beta_0^{(s)} &\sim \text{Normal}\left(\beta_0^{(s),\text{true}}, 0.001^2\right) \\
\beta_x^{(s)} &\sim \text{TruncatedNormal}\left(\beta_x^{(s),\text{true}}, 0.001^2, 0, +\infty\right) \\
\beta_0^{(g)} &\sim \text{Normal}\left(\beta_0^{(g),\text{true}}, 0.001^2\right) \\
\beta_x^{(g)} &\sim \text{TruncatedNormal}\left(\beta_x^{(g),\text{true}}, 0.001^2, 0, +\infty\right) \\
\sigma^{(g)} &\sim \text{Uniform}\left(0.999\sigma^{(g),\text{true}}, 1.001\sigma^{(g),\text{true}}\right) \\
\beta_0^{(f)} &\sim \text{Normal}\left(\beta_0^{(f),\text{true}}, 0.001^2\right) \\
\eta^{(r)} &\sim \text{Uniform}\left(0.999\eta^{(r),\text{true}}, 1.001\eta^{(r),\text{true}}\right)
\end{aligned} \tag{36}$$

2. Vague priors on survival parameters and tight priors on others.

$$
\begin{aligned}
\beta_0^{(s)} &\sim \text{Normal}\left(0, 5^2\right) \\
\beta_x^{(s)} &\sim \text{TruncatedNormal}\left(0, 5^2, 0, +\infty\right) \\
\beta_0^{(g)} &\sim \text{Normal}\left(\beta_0^{(g),\text{true}}, 0.001^2\right) \\
\beta_x^{(g)} &\sim \text{TruncatedNormal}\left(\beta_x^{(g),\text{true}}, 0.001^2, 0, +\infty\right) \\
\sigma^{(g)} &\sim \text{Uniform}\left(0.999\sigma^{(g),\text{true}}, 1.001\sigma^{(g),\text{true}}\right) \\
\beta_0^{(f)} &\sim \text{Normal}\left(\beta_0^{(f),\text{true}}, 0.001^2\right) \\
\eta^{(r)} &\sim \text{Uniform}\left(0.999\eta^{(r),\text{true}}, 1.001\eta^{(r),\text{true}}\right)
\end{aligned}
\qquad 37
$$

3. Vague priors on growth parameters and tight priors on others.

$$
\begin{aligned}
\beta_0^{(s)} &\sim \text{Normal}\left(\beta_0^{(s),\text{true}}, 0.001^2\right) \\
\beta_x^{(s)} &\sim \text{TruncatedNormal}\left(\beta_x^{(s),\text{true}}, 0.001^2, 0, +\infty\right) \\
\beta_0^{(g)} &\sim \text{Normal}\left(0, 5^2\right) \\
\beta_x^{(g)} &\sim \text{TruncatedNormal}\left(0, 5^2, 0, +\infty\right) \\
\sigma^{(g)} &\sim \text{Uniform}\left(0, 5\right) \\
\beta_0^{(f)} &\sim \text{Normal}\left(\beta_0^{(f),\text{true}}, 0.001^2\right) \\
\eta^{(r)} &\sim \text{Uniform}\left(0.999\eta^{(r),\text{true}}, 1.001\eta^{(r),\text{true}}\right)
\end{aligned}
\qquad 38
$$

4. Vague priors on fecundity parameter and tight priors on others.

$$
\begin{aligned}
\beta_0^{(s)} &\sim \text{Normal}\left(\beta_0^{(s),\text{true}}, 0.001^2\right) \\
\beta_x^{(s)} &\sim \text{TruncatedNormal}\left(\beta_x^{(s),\text{true}}, 0.001^2, 0, +\infty\right) \\
\beta_0^{(g)} &\sim \text{Normal}\left(\beta_0^{(g),\text{true}}, 0.001^2\right) \\
\beta_x^{(g)} &\sim \text{TruncatedNormal}\left(\beta_x^{(g),\text{true}}, 0.001^2, 0, +\infty\right) \\
\sigma^{(g)} &\sim \text{Uniform}\left(0.999\sigma^{(g),\text{true}}, 1.001\sigma^{(g),\text{true}}\right) \\
\beta_0^{(f)} &\sim \text{Normal}\left(0, 5^2\right) \\
\eta^{(r)} &\sim \text{Uniform}\left(0.999\eta^{(r),\text{true}}, 1.001\eta^{(r),\text{true}}\right)
\end{aligned}
\tag{39}
$$

5. Vague priors on recruitment parameter and tight priors on others.

$$
\begin{aligned}
\beta_0^{(s)} &\sim \text{Normal}\left(\beta_0^{(s),\text{true}}, 0.001^2\right) \\
\beta_x^{(s)} &\sim \text{TruncatedNormal}\left(\beta_x^{(s),\text{true}}, 0.001^2, 0, +\infty\right) \\
\beta_0^{(g)} &\sim \text{Normal}\left(\beta_0^{(g),\text{true}}, 0.001^2\right) \\
\beta_x^{(g)} &\sim \text{TruncatedNormal}\left(\beta_x^{(g),\text{true}}, 0.001^2, 0, +\infty\right) \\
\sigma^{(g)} &\sim \text{Uniform}\left(0.999\sigma^{(g),\text{true}}, 1.001\sigma^{(g),\text{true}}\right) \\
\beta_0^{(f)} &\sim \text{Normal}\left(\beta_0^{(f),\text{true}}, 0.001^2\right) \\
\eta^{(r)} &\sim \text{Uniform}\left(0, 50\right)
\end{aligned}
\tag{40}
$$

Parameter posterior distributions are simulated using Markov chain Monte Carlo (MCMC) with 100,000 iterations, discarding the first 5,000 iterations as burn-in, and thinning each 20th iterations. Convergence is checked by visually assessing trace plots and correlation plots (pairs) of the MCMC chains.

Under all prior specifications, all simulations can well predict population size distributions (e.g., Figure 2) and population sizes (e.g., Figure 3). However, parameter

estimations are challenging except the case with tight priors on all parameters (Equation 36). The sensitivity corresponds to the change of stable stage distribution w.r.t. each parameter. The subsequent figures show true, prior, posterior parameter comparisons and sensitivities.

Simulation 1—Posteriors can recover to true parameters under tight priors (Equation 36; Figure 7), but not vague priors (Equations 37 – 40; Figures 8 – 11). In general, sensitivities are greatest for the growth component, especially under vague prior on fecundity (Equation 39; Figure 10). Furthermore, sensitivities drop at small size classes, increase at medium size classes, and somewhat drop again at large size classes (e.g., Figure 7), except an abrupt change in growth sensitivity under vague prior on growth (Equation 38; Figure 9).

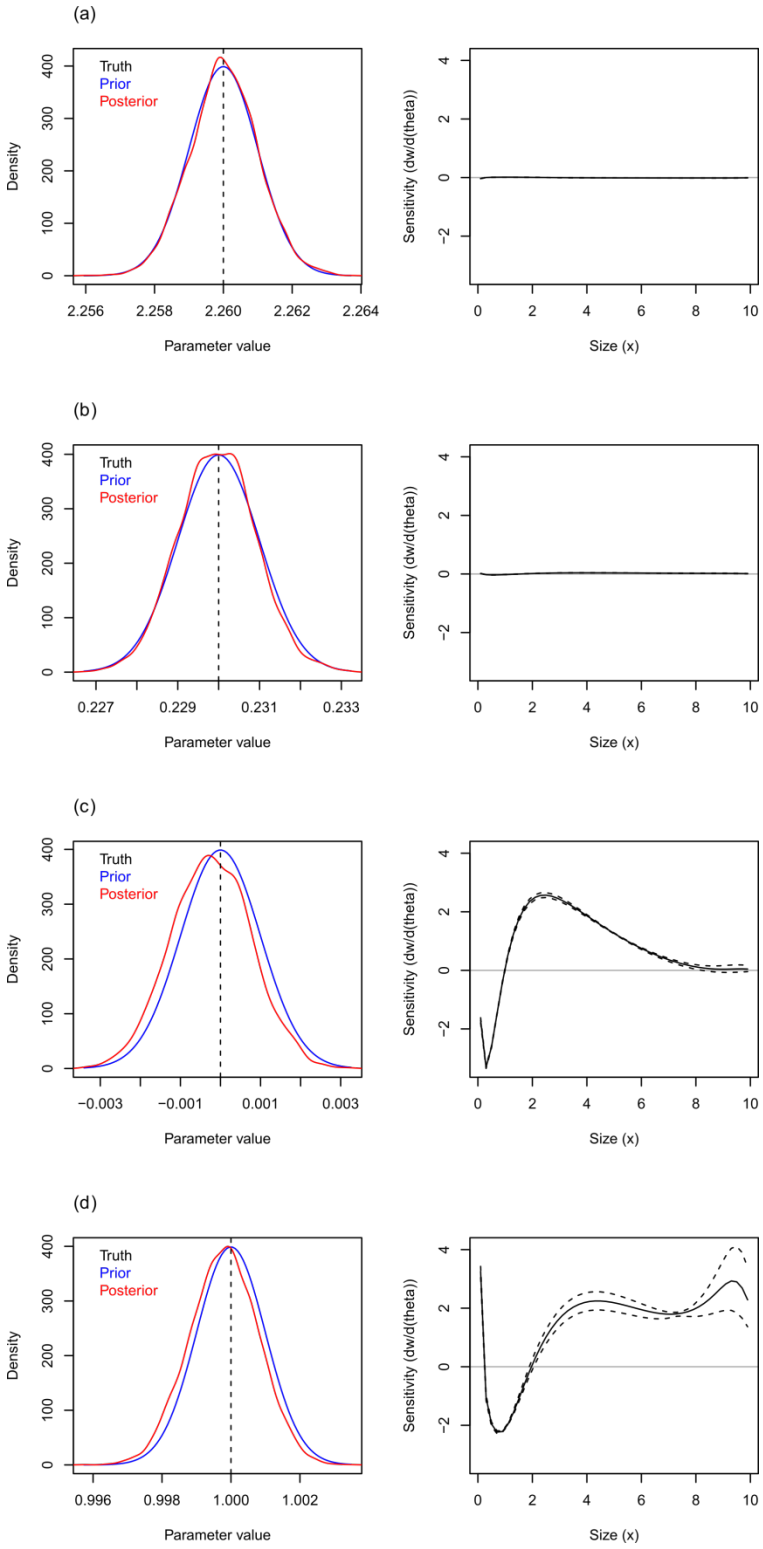
(a)
Truth
Prior
Posterior
Density
Parameter value
Sensitivity (dw/d(theta))
Size (x)
(b)
Truth
Prior
Posterior
Density
Parameter value
Sensitivity (dw/d(theta))
Size (x)
(c)
Truth
Prior
Posterior
Density
Parameter value
Sensitivity (dw/d(theta))
Size (x)
(d)
Truth
Prior
Posterior
Density
Parameter value
Sensitivity (dw/d(theta))
Size (x)

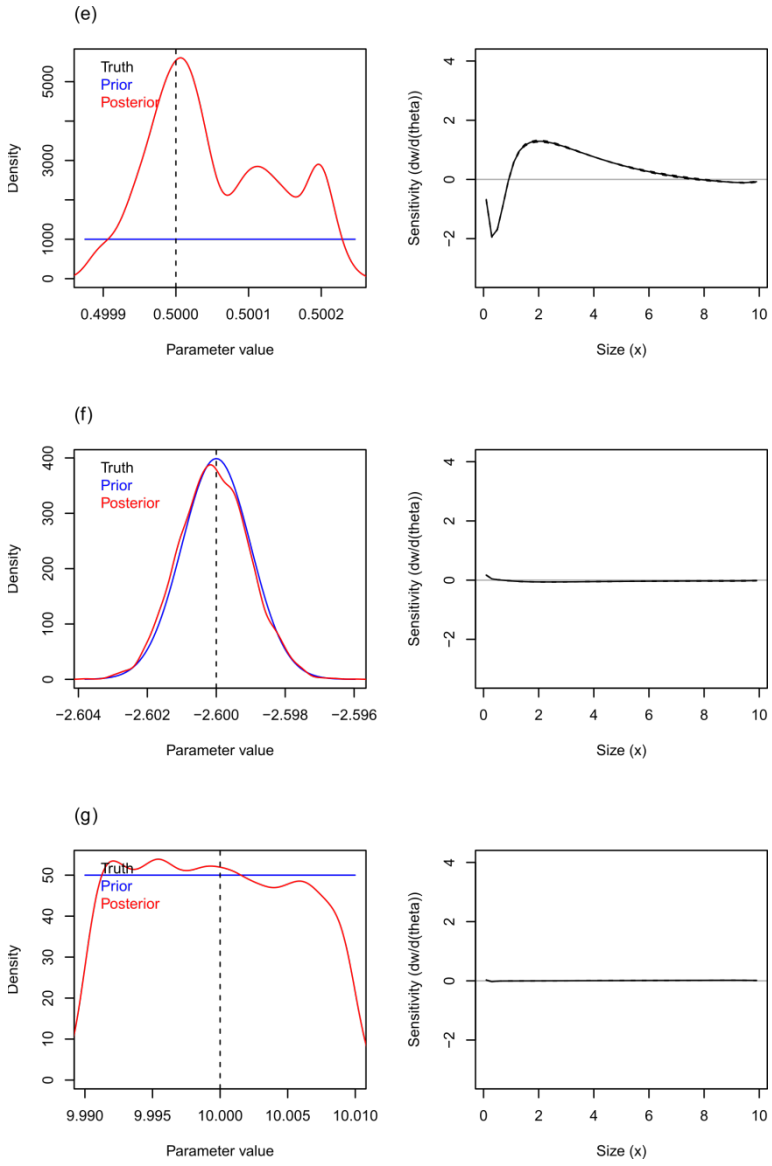

Figure 7: Simulation 1 with tight priors on all parameters (Equation 36). Left: true (black), prior (blue), and posterior (red) parameter (θ) comparisons. Right: sensitivity of stable stage distribution to parameters ($dw/d\theta$, posterior mean: solid; 95% credible intervals: dashed lines). Panels are (a) survival parameter $\beta_0^{(s)}$; (b) survival parameter $\beta_x^{(s)}$; (c) growth parameter $\beta_0^{(g)}$; (d) growth parameter $\beta_x^{(g)}$; (e) growth parameter $\sigma^{(g)}$; (f) fecundity parameter $\beta_0^{(f)}$; and (g) recruitment parameter $\eta^{(r)}$.

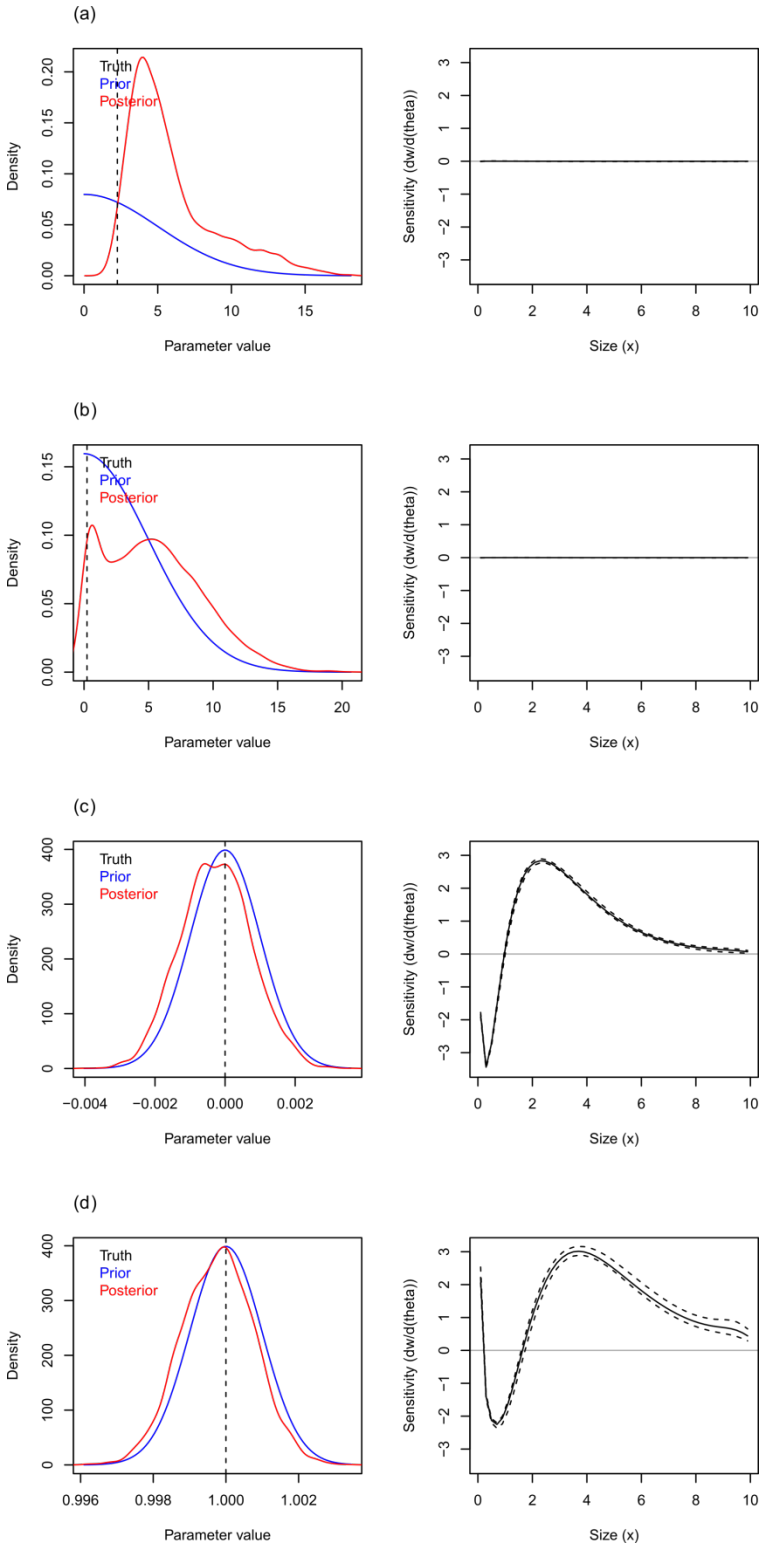
(a)
Truth
Prior
Posterior
Density
Parameter value
Sensitivity (dw/d(theta))
Size (x)
(b)
Truth
Prior
Posterior
Density
Parameter value
Sensitivity (dw/d(theta))
Size (x)
(c)
Truth
Prior
Posterior
Density
Parameter value
Sensitivity (dw/d(theta))
Size (x)
(d)
Truth
Prior
Posterior
Density
Parameter value
Sensitivity (dw/d(theta))
Size (x)

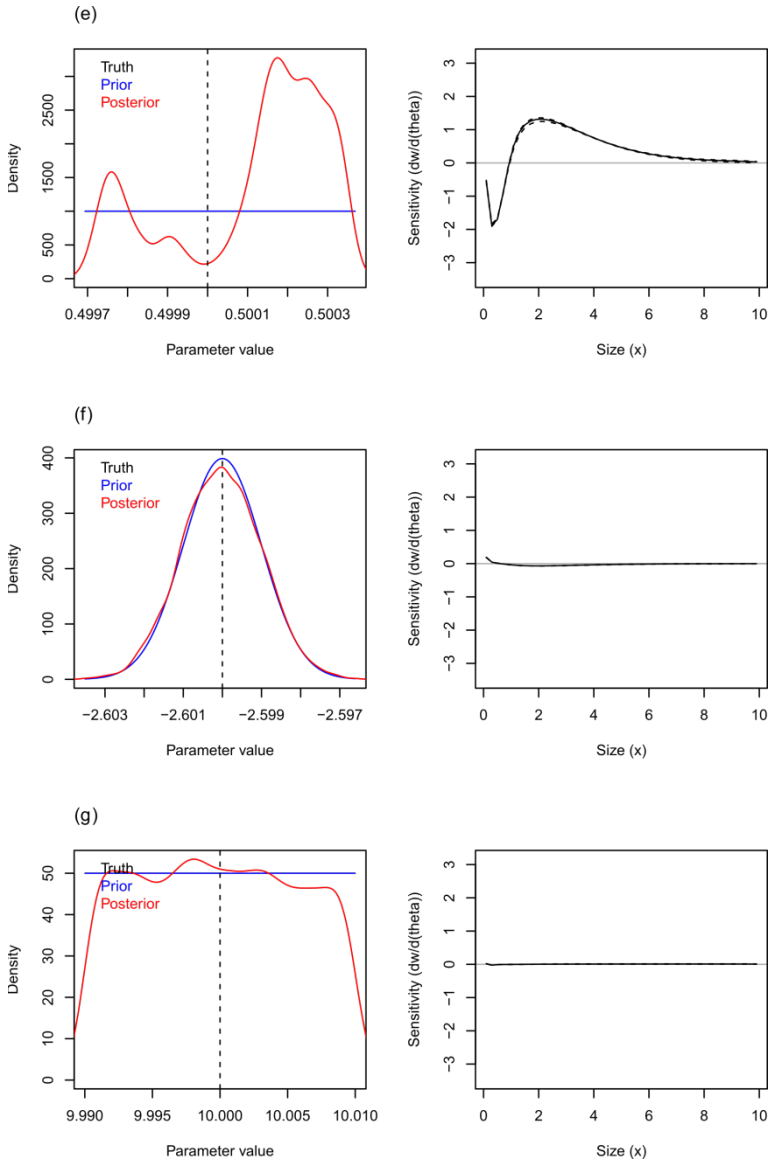

Figure 8: Simulation 1 with vague priors on survival parameters and tight priors on others (Equation 37). Symbolism follows Figure 7.

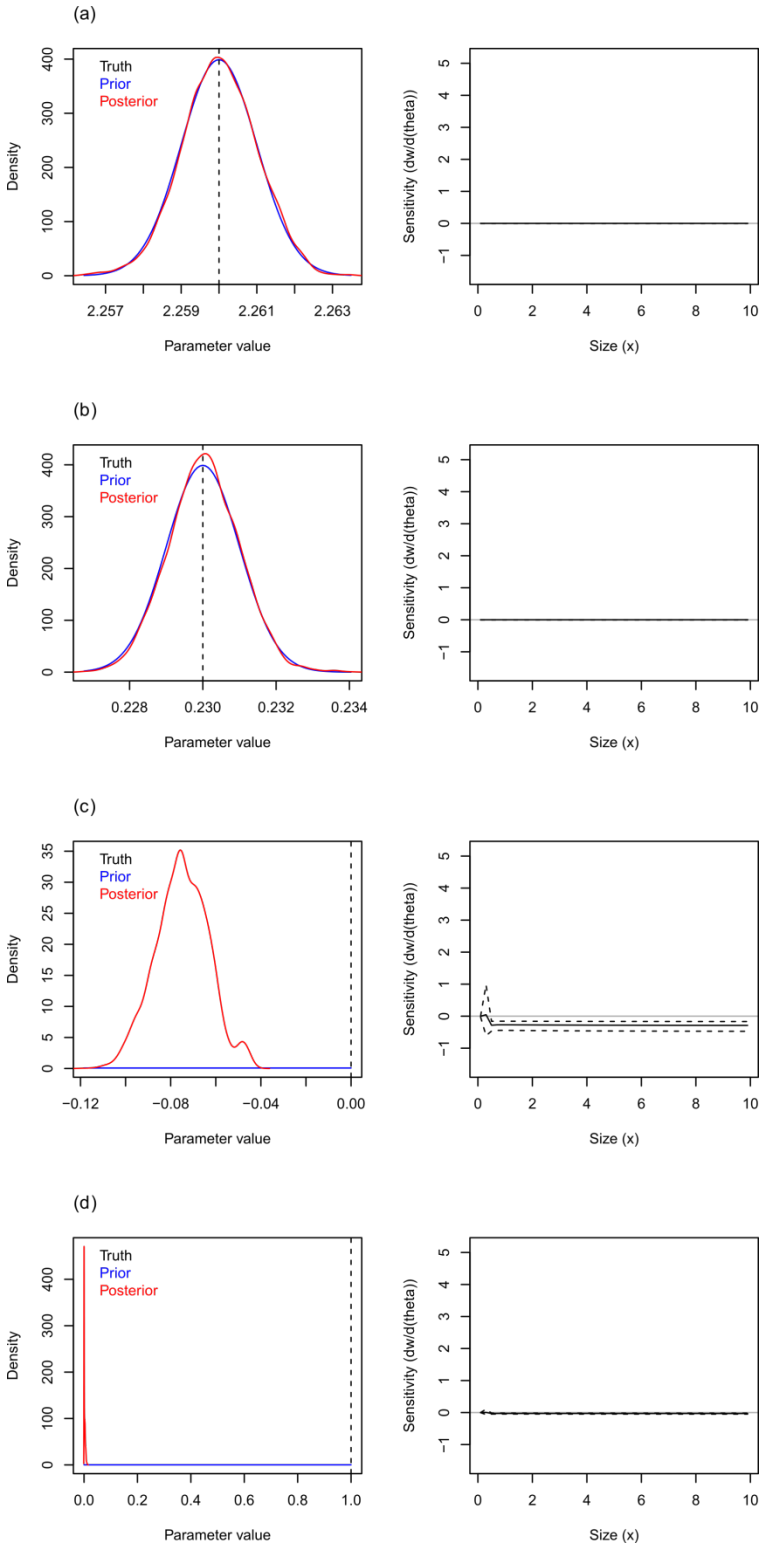
(a)
Truth
Prior
Posterior
Density
Parameter value
Sensitivity (dw/d(theta))
Size (x)
(b)
Truth
Prior
Posterior
Density
Parameter value
Sensitivity (dw/d(theta))
Size (x)
(c)
Truth
Prior
Posterior
Density
Parameter value
Sensitivity (dw/d(theta))
Size (x)
(d)
Truth
Prior
Posterior
Density
Parameter value
Sensitivity (dw/d(theta))
Size (x)

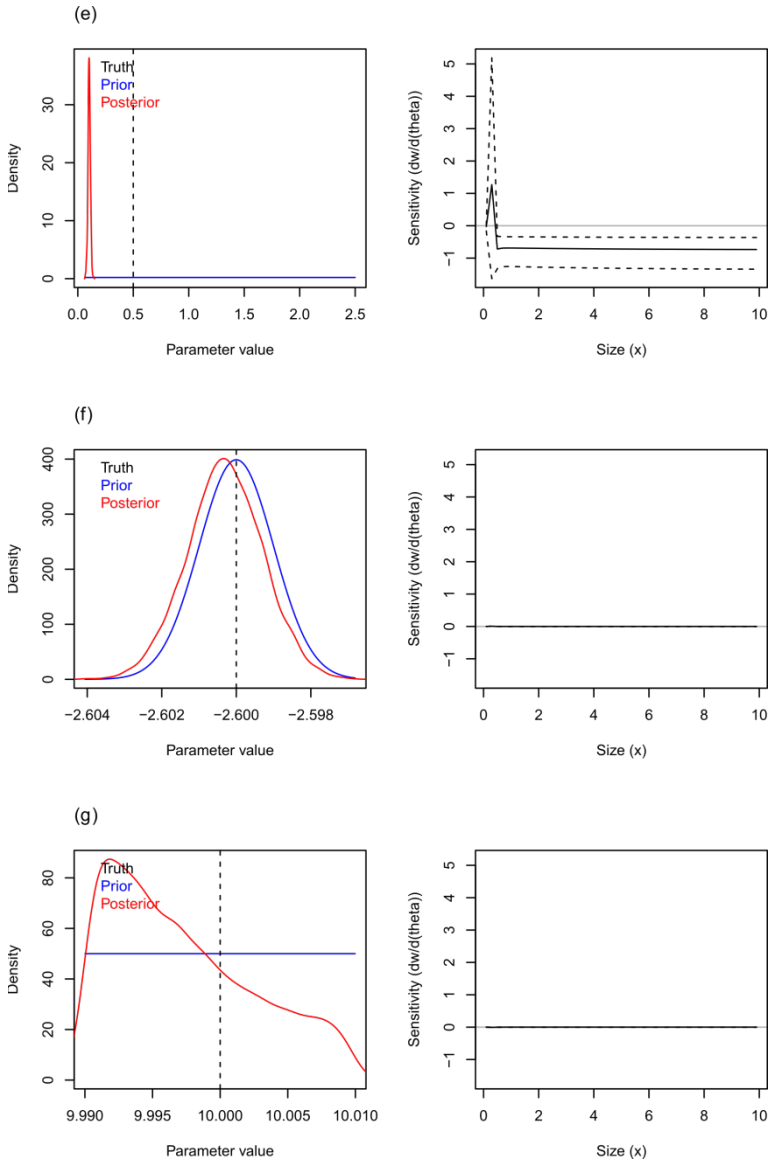

Figure 9: Simulation 1 with vague priors on growth parameters and tight priors on others (Equation 38). Symbolism follows Figure 7.

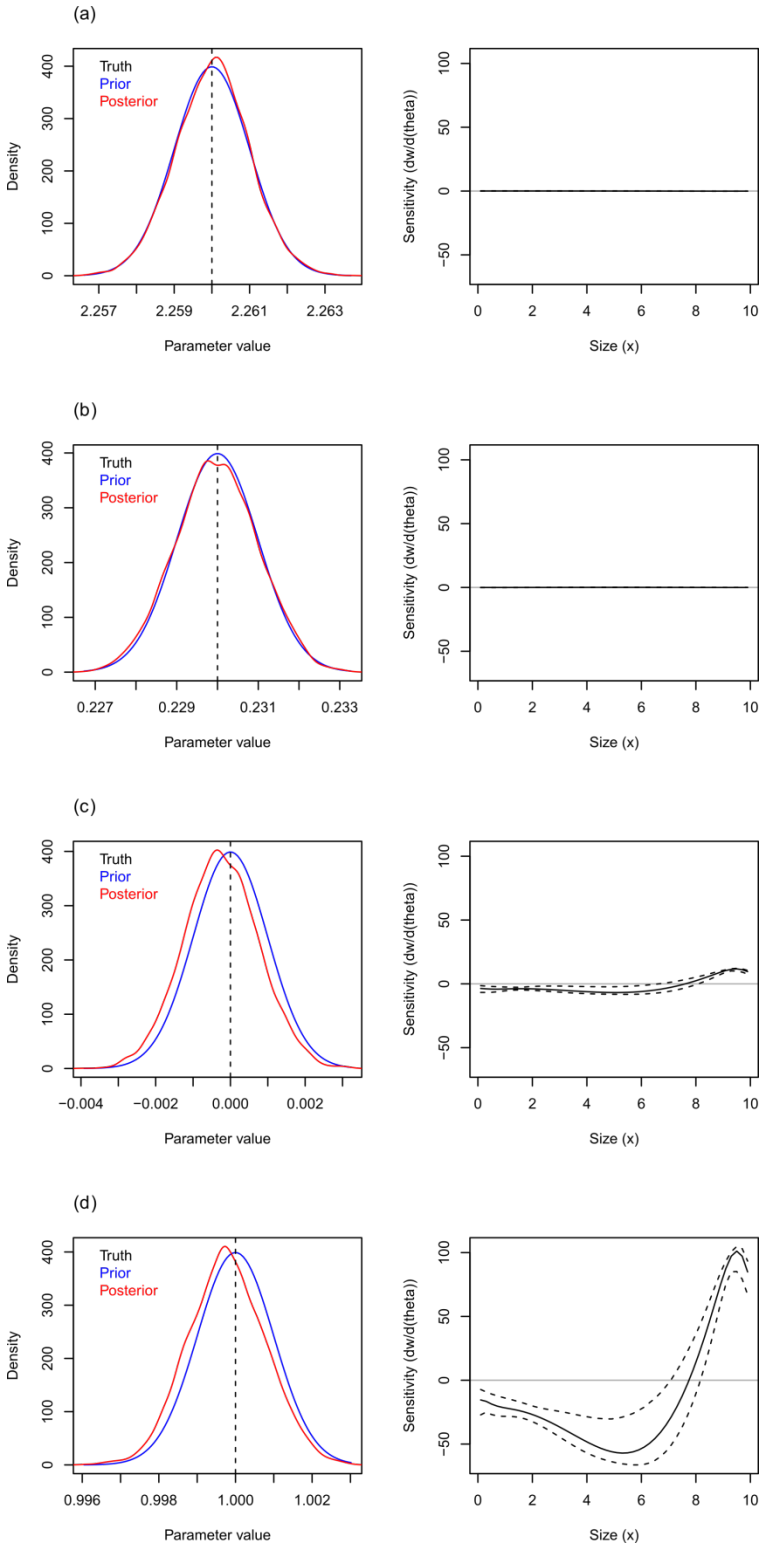
(a)
Truth
Prior
Posterior
Density
Parameter value
Sensitivity (dw/d(theta))
Size (x)
(b)
Truth
Prior
Posterior
Density
Parameter value
Sensitivity (dw/d(theta))
Size (x)
(c)
Truth
Prior
Posterior
Density
Parameter value
Sensitivity (dw/d(theta))
Size (x)
(d)
Truth
Prior
Posterior
Density
Parameter value
Sensitivity (dw/d(theta))
Size (x)

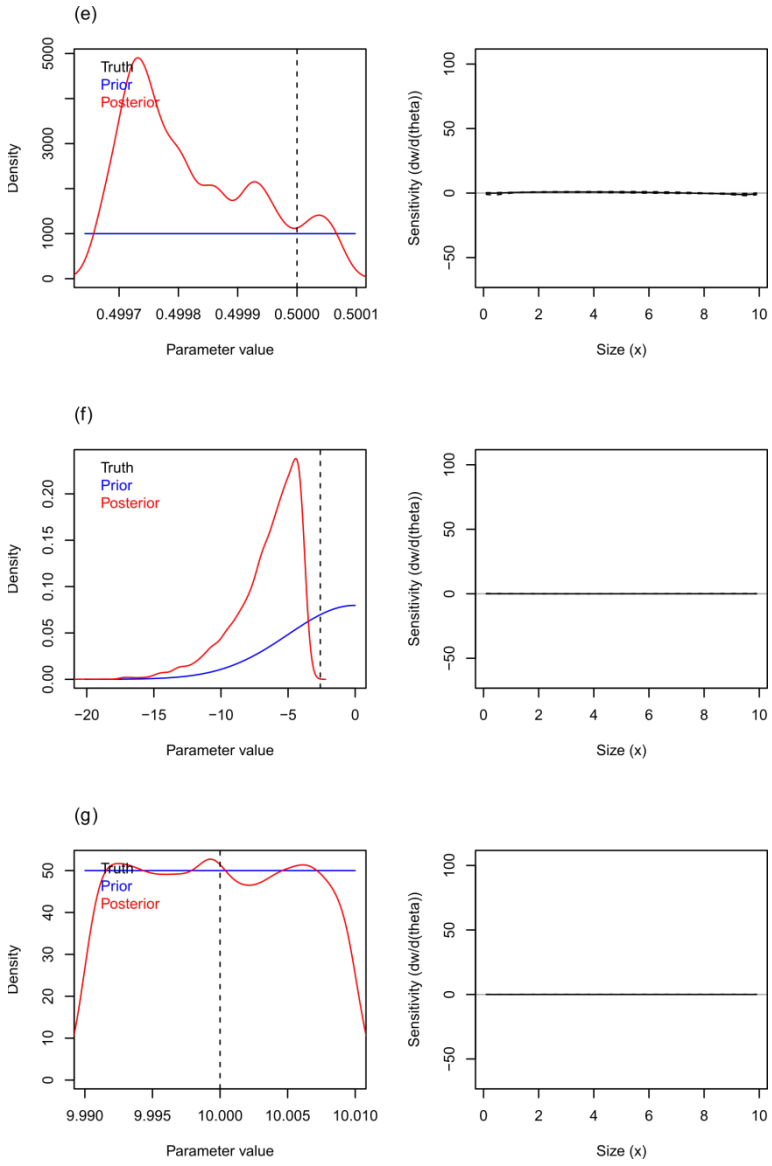

Figure 10: Simulation 1 with vague priors on fecundity parameter and tight priors on others (Equation 39). Symbolism follows Figure 7.

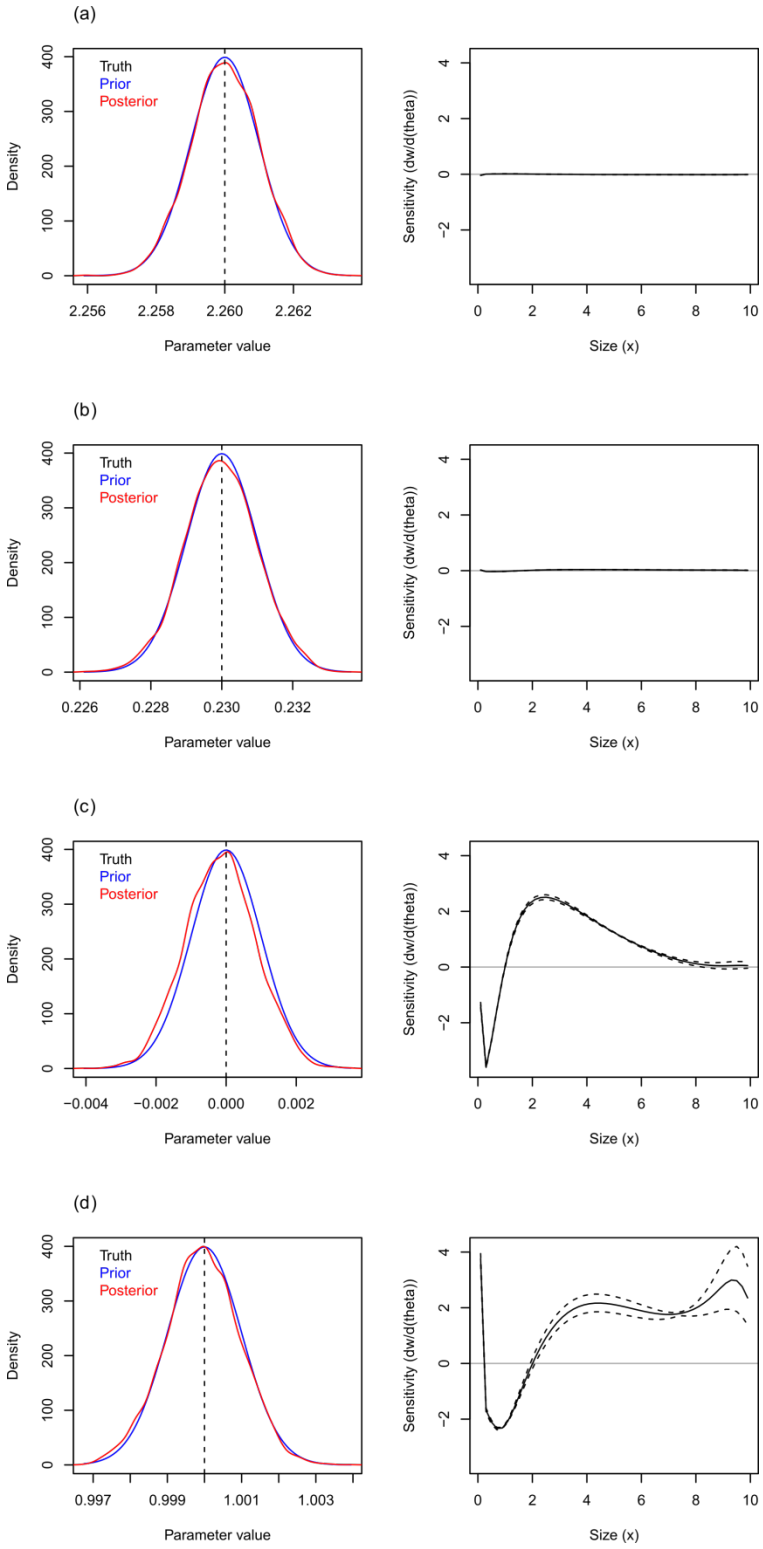
(a)
Truth
Prior
Posterior
Density
Parameter value
Sensitivity (dw/d(theta))
Size (x)
(b)
Truth
Prior
Posterior
Density
Parameter value
Sensitivity (dw/d(theta))
Size (x)
(c)
Truth
Prior
Posterior
Density
Parameter value
Sensitivity (dw/d(theta))
Size (x)
(d)
Truth
Prior
Posterior
Density
Parameter value
Sensitivity (dw/d(theta))
Size (x)

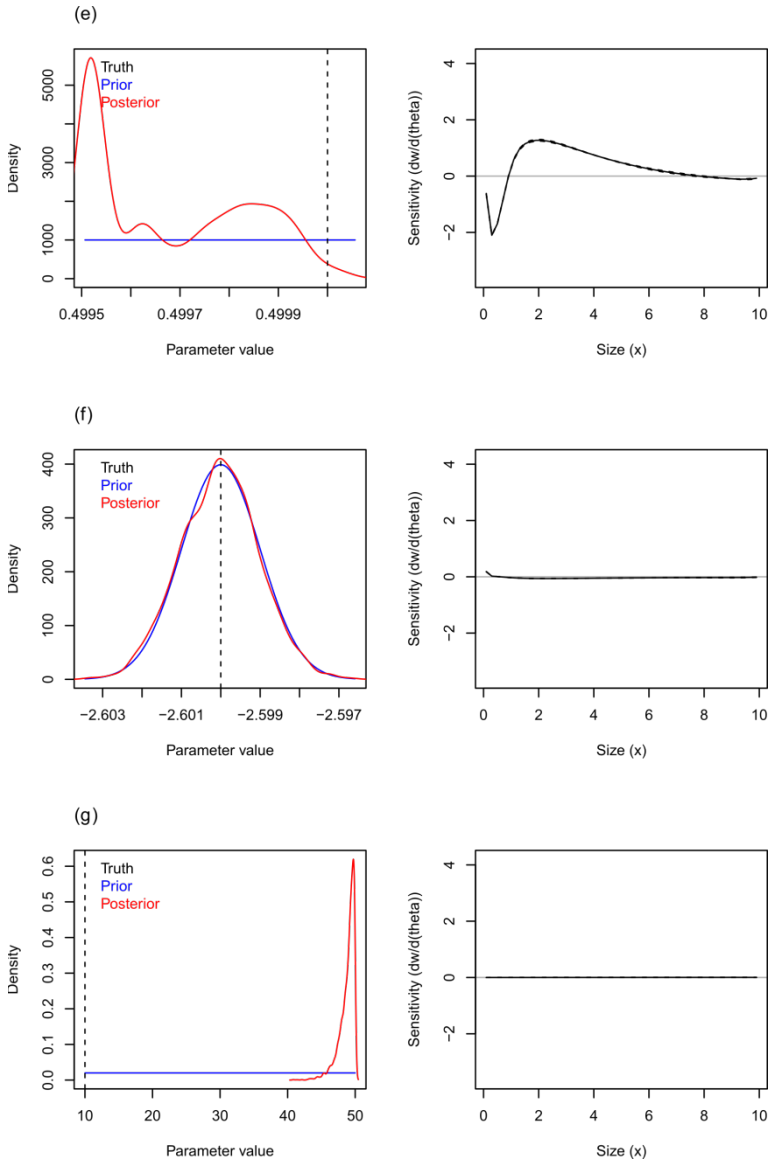

Figure 11: Simulation 1 with vague priors on recruitment parameter and tight priors on others (Equation 40). Symbolism follows Figure 7.

Simulation 2——Posteriors can recover to true parameters under tight priors (Equation 36; Figure 12), but not vague priors (Equations 37 – 40; Figures 13 – 16). In general, sensitivities are greatest for the growth component (e.g., Figure 12). The sensitivity to survival is also appreciable under vague priors on survival (Equation 37; Figure 8). The sensitivity to growth has

oscillation patterns from small to large size classes (Figures 12, 13, 15, and 16), except an abrupt change in growth sensitivity under vague prior on growth (Equation 38; Figure 14).

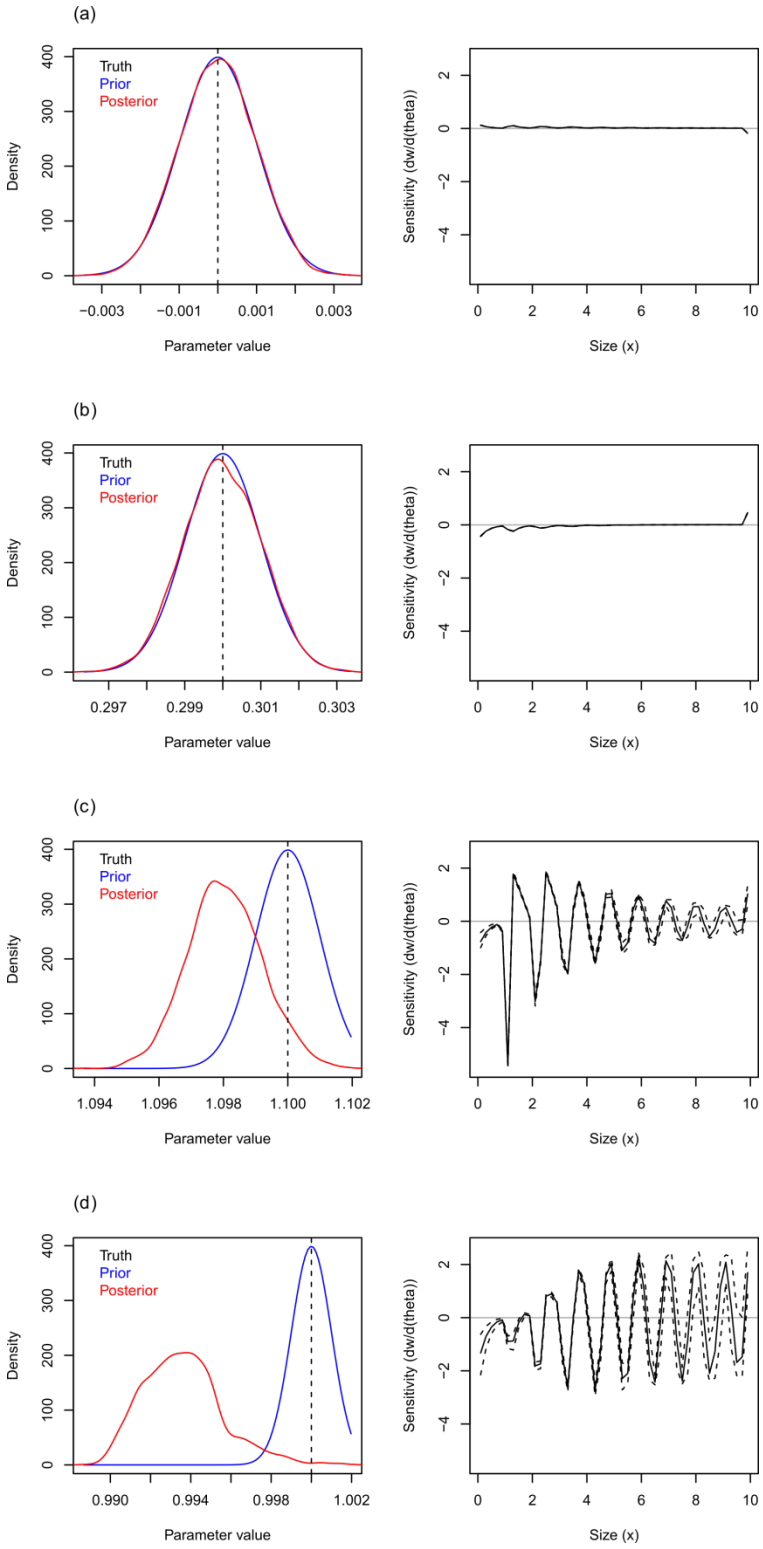
(a)
Truth
Prior
Posterior
Density
Parameter value
Sensitivity (dw/d(theta))
Size (x)
(b)
Truth
Prior
Posterior
Density
Parameter value
Sensitivity (dw/d(theta))
Size (x)
(c)
Truth
Prior
Posterior
Density
Parameter value
Sensitivity (dw/d(theta))
Size (x)
(d)
Truth
Prior
Posterior
Density
Parameter value
Sensitivity (dw/d(theta))
Size (x)

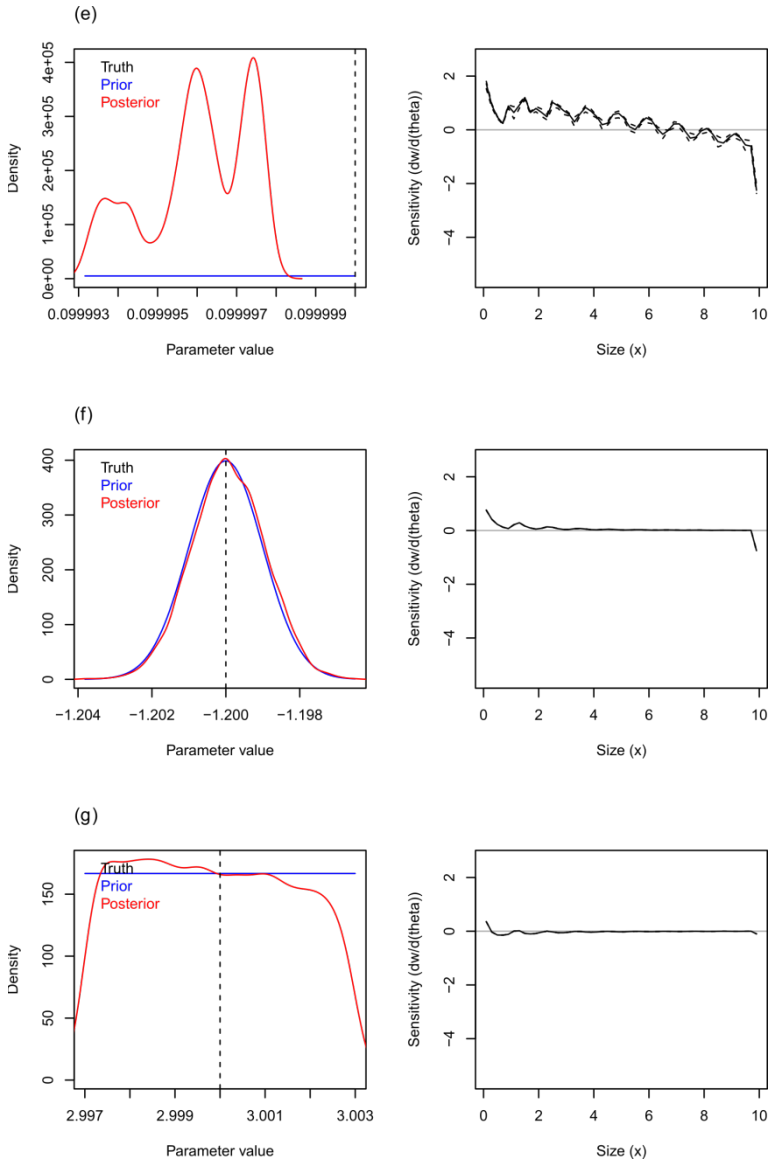

Figure 12: Simulation 2 with tight priors on all parameters (Equation 36). Symbolism follows Figure 7.

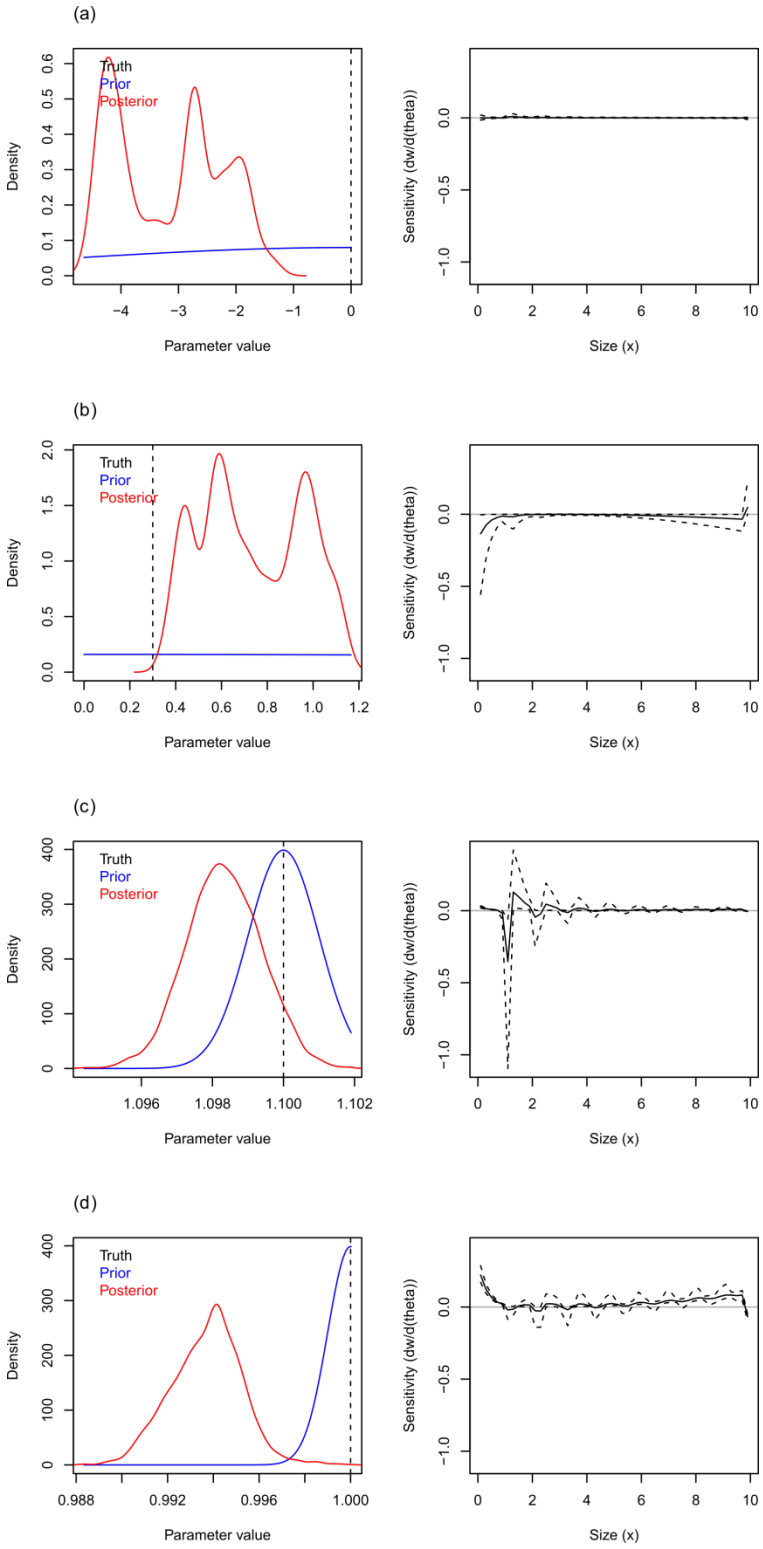
(a)
Truth
Prior
Posterior
Density
Parameter value
Sensitivity (dw/d(theta))
Size (x)
(b)
Truth
Prior
Posterior
Density
Parameter value
Sensitivity (dw/d(theta))
Size (x)
(c)
Truth
Prior
Posterior
Density
Parameter value
Sensitivity (dw/d(theta))
Size (x)
(d)
Truth
Prior
Posterior
Density
Parameter value
Sensitivity (dw/d(theta))
Size (x)

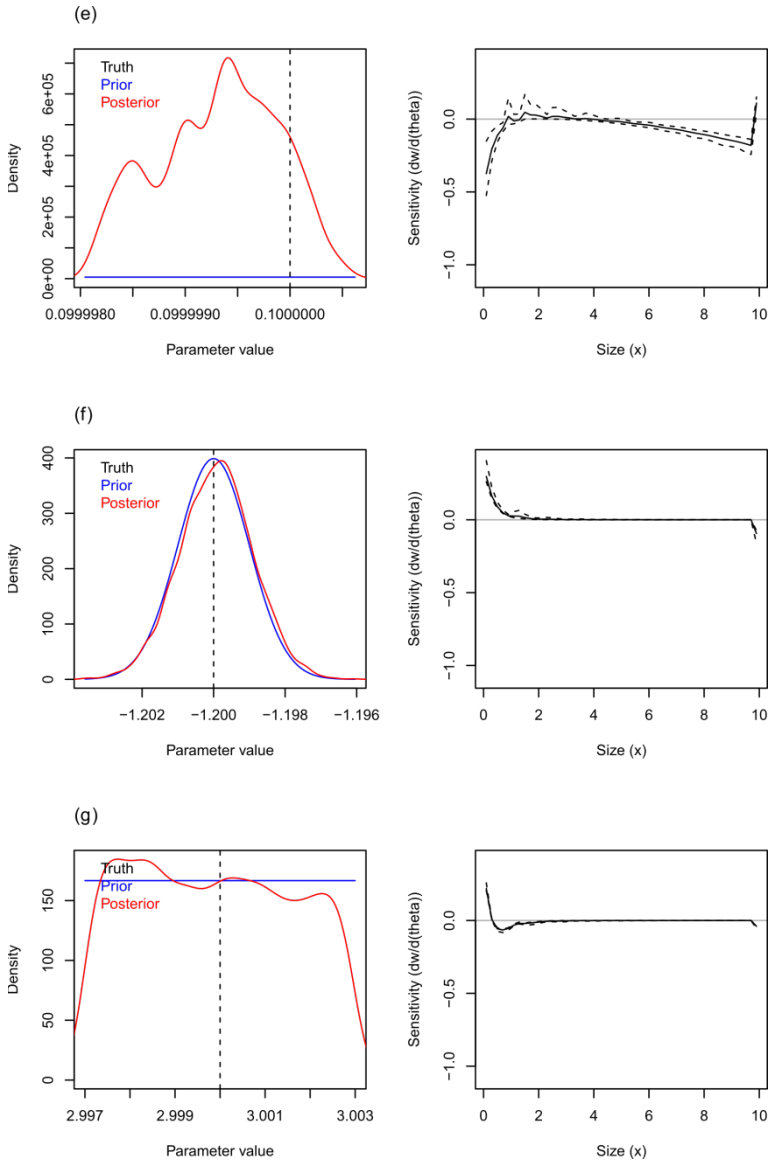

Figure 13: Simulation 2 with vague priors on survival parameters and tight priors on others (Equation 37). Symbolism follows Figure 7.

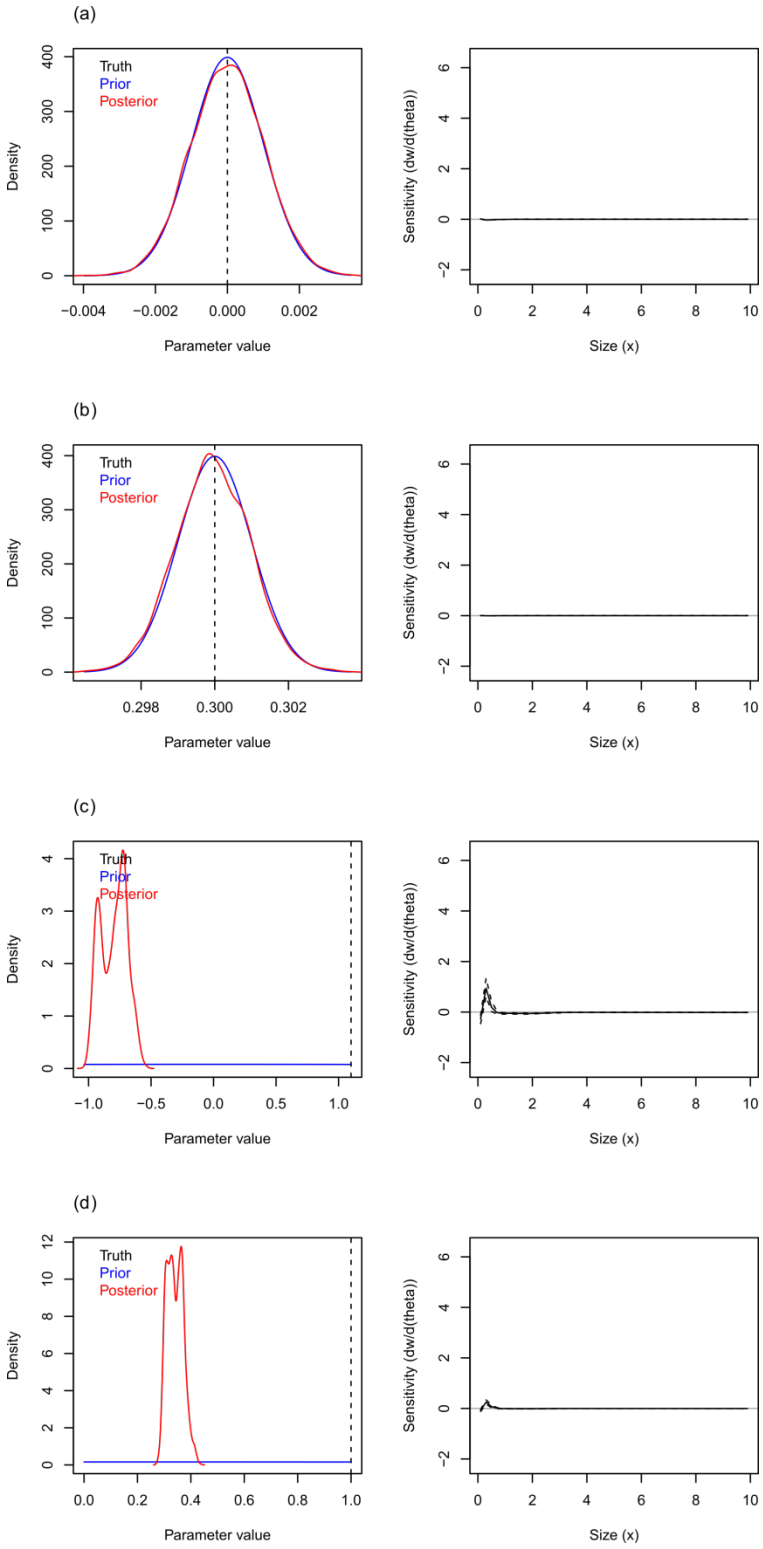
(a)
Truth
Prior
Posterior
Density
Parameter value
Sensitivity (dw/d(theta))
Size (x)
(b)
Truth
Prior
Posterior
Density
Parameter value
Sensitivity (dw/d(theta))
Size (x)
(c)
Truth
Prior
Posterior
Density
Parameter value
Sensitivity (dw/d(theta))
Size (x)
(d)
Truth
Prior
Posterior
Density
Parameter value
Sensitivity (dw/d(theta))
Size (x)

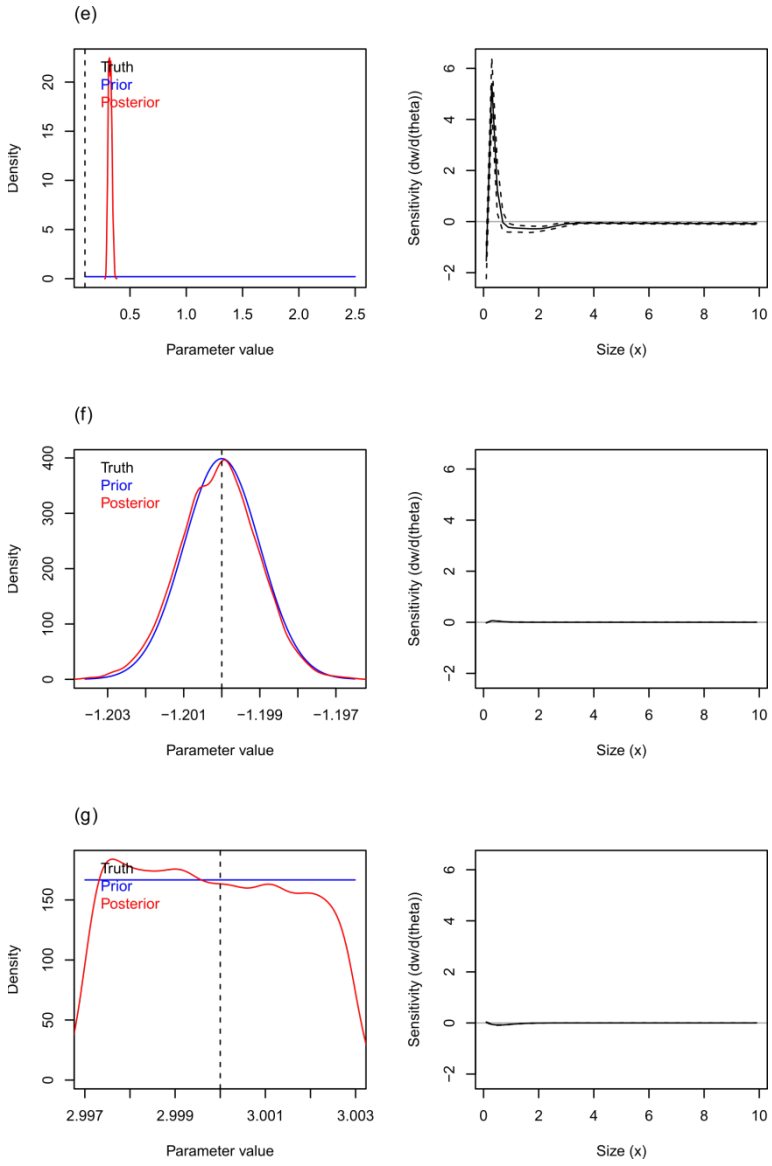

Figure 14: Simulation 2 with vague priors on growth parameters and tight priors on others (Equation 38). Symbolism follows Figure 7.

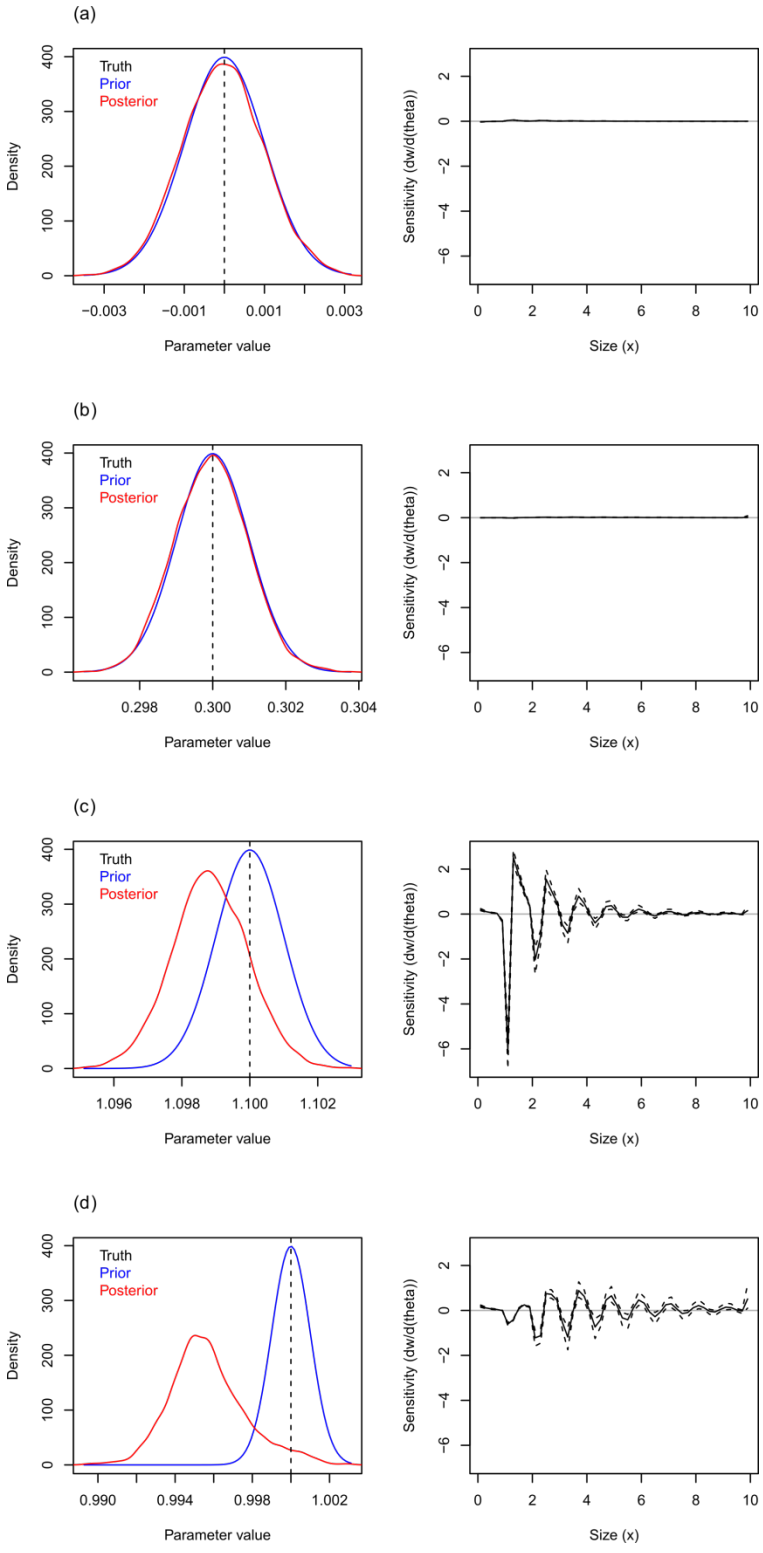
(a)
Truth
Prior
Posterior
Density
Parameter value
Sensitivity (dw/d(theta))
Size (x)
(b)
Truth
Prior
Posterior
Density
Parameter value
Sensitivity (dw/d(theta))
Size (x)
(c)
Truth
Prior
Posterior
Density
Parameter value
Sensitivity (dw/d(theta))
Size (x)
(d)
Truth
Prior
Posterior
Density
Parameter value
Sensitivity (dw/d(theta))
Size (x)

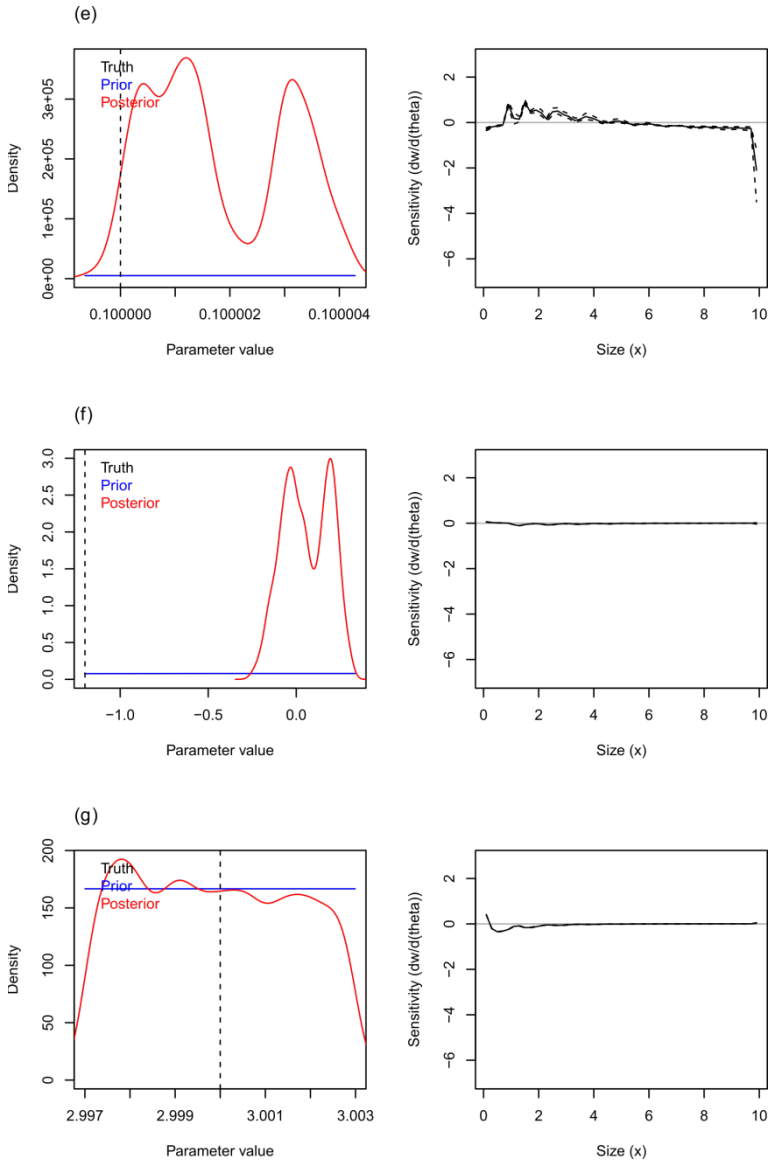

Figure 15: Simulation 2 with vague priors on fecundity parameter and tight priors on others (Equation 39). Symbolism follows Figure 7.

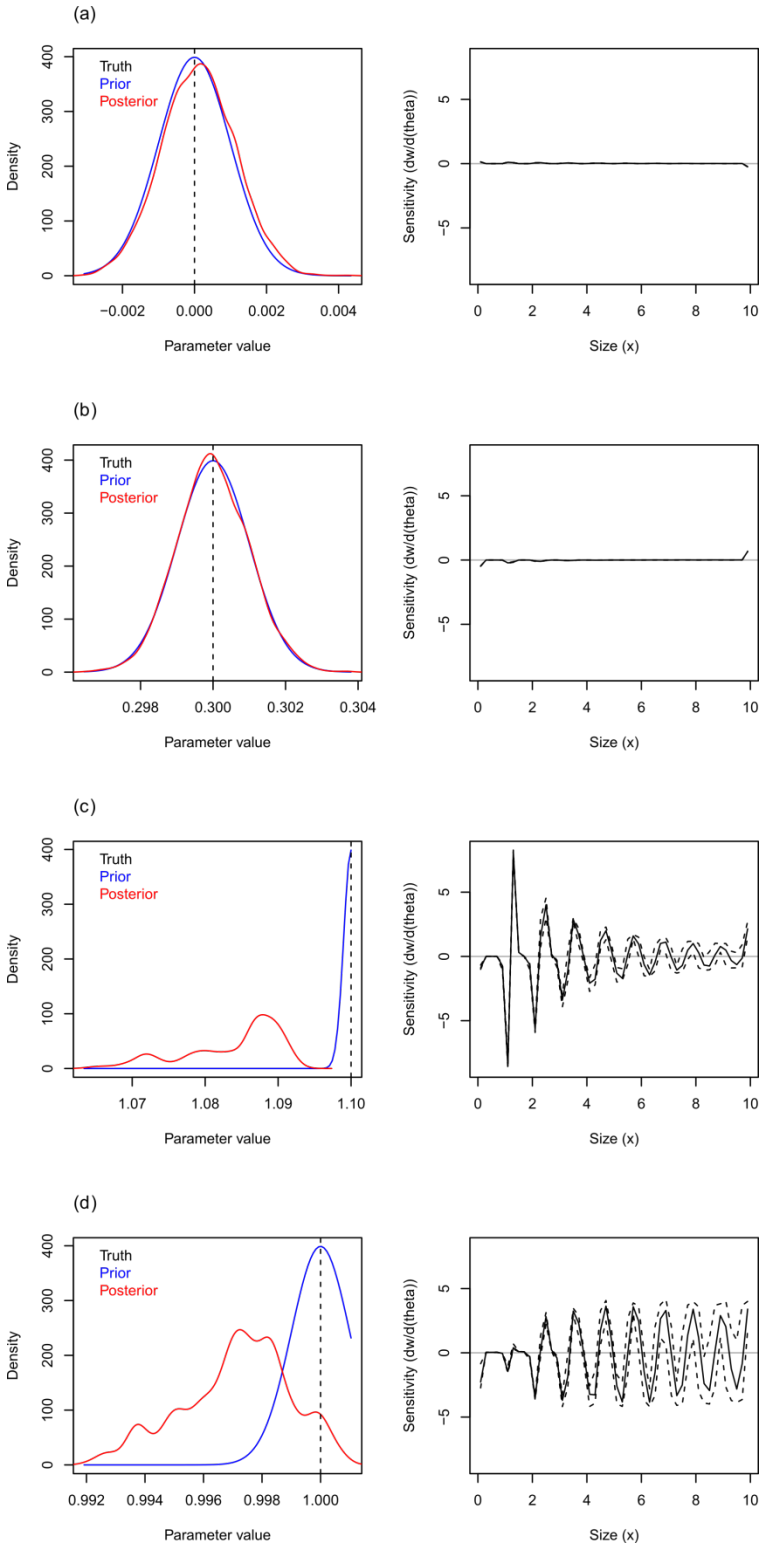
(a)
Truth
Prior
Posterior
Density
Parameter value
Sensitivity (dw/d(theta))
Size (x)
(b)
Truth
Prior
Posterior
Density
Parameter value
Sensitivity (dw/d(theta))
Size (x)
(c)
Truth
Prior
Posterior
Density
Parameter value
Sensitivity (dw/d(theta))
Size (x)
(d)
Truth
Prior
Posterior
Density
Parameter value
Sensitivity (dw/d(theta))
Size (x)

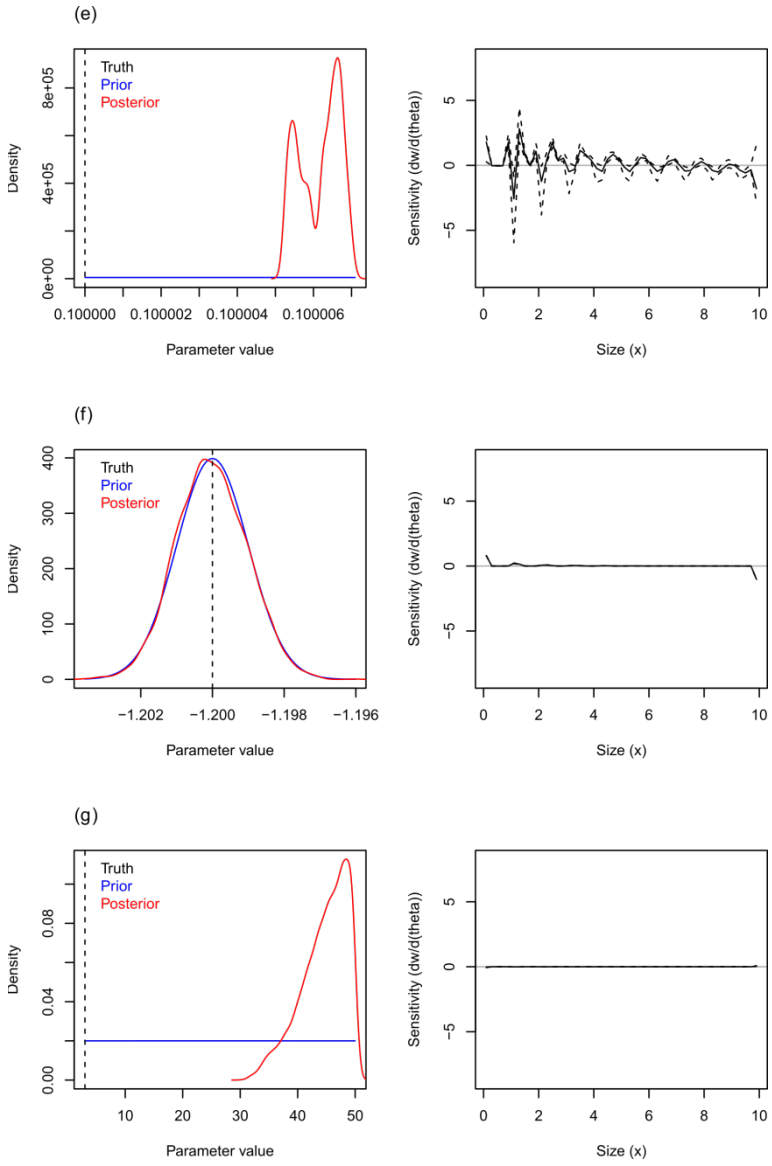

Figure 16: Simulation 2 with vague priors on recruitment parameter and tight priors on others (Equation 40). Symbolism follows Figure 7.

1.5 Summary and future works

We have presented simulation studies and sensitivity analyses to explore the properties of the new population-level IPM (PIPM). The simulation studies show that parameter recovery is challenging, suggesting possible parameter identification problems. The sensitivity analyses,

however, could somewhat help to uncover the problems by identifying parameters that are most sensitive to the stable stage distributions. Taken together, we find that for population-level only data, information may be limited to infer demography. Future works will see the integration of both individual- and population-level information to benefit population dynamics and demography modeling.

References

Caswell H (2001) *Matrix Population Models: Construction, Analysis, and Interpretation,* Sunderland, MA., Sinauer Associates.

Dalgleish HJ, Koons DN, Hooten MB, Moffet CA, Adler PB (2011) Climate influences the demography of three dominant sagebrush steppe plants. *Ecology,* **92**, 75-85.

Easterling MR, Ellner SP, Dixon PM (2000) Size-specific sensitivity: applying a new structured population model. *Ecology,* **81**, 694-708.

Ellner SP, Rees M (2006) Integral projection models for species with complex demography. *American Naturalist,* **167**, 410-428.

Ellner SP, Rees M (2009) Integral projection models for populations in temporally varying environments. *Ecological Monographs,* **79**, 575-594.

Ghosh S, Gelfand AE, Clark JS (2012) Inference for size demography from point pattern data using integral projection models. *Journal of Agricultural, Biological and Environmental Statistics,* **17**, 641-677.

Lewis PAW, Shedler GS (1979) Simulation of nonhomogeneous Poisson processes by thinning. *Naval Research Logistics,* **26**, 403-413.

R Development Core Team (2013) R: A language and environment for statistical computing. R Foundation for Statistical Computing, Vienna, Austria. http://www.R-project.org